

A non-canonical tricarboxylic acid cycle underlies cellular identity

<https://doi.org/10.1038/s41586-022-04475-w>

Received: 19 February 2021

Accepted: 26 January 2022

Published online: 9 March 2022

 Check for updates

Paige K. Arnold^{1,2,6}, Benjamin T. Jackson^{1,2,6}, Katrina I. Paras^{1,3}, Julia S. Brunner¹, Madeleine L. Hart⁴, Oliver J. Newsom⁴, Sydney P. Alibekoff⁴, Jennifer Endress^{1,3}, Esther Drill⁵, Lucas B. Sullivan⁴ & Lydia W. S. Finley¹✉

The tricarboxylic acid (TCA) cycle is a central hub of cellular metabolism, oxidizing nutrients to generate reducing equivalents for energy production and critical metabolites for biosynthetic reactions. Despite the importance of the products of the TCA cycle for cell viability and proliferation, mammalian cells display diversity in TCA-cycle activity^{1,2}. How this diversity is achieved, and whether it is critical for establishing cell fate, remains poorly understood. Here we identify a non-canonical TCA cycle that is required for changes in cell state. Genetic co-essentiality mapping revealed a cluster of genes that is sufficient to compose a biochemical alternative to the canonical TCA cycle, wherein mitochondrially derived citrate exported to the cytoplasm is metabolized by ATP citrate lyase, ultimately regenerating mitochondrial oxaloacetate to complete this non-canonical TCA cycle. Manipulating the expression of ATP citrate lyase or the canonical TCA-cycle enzyme aconitase 2 in mouse myoblasts and embryonic stem cells revealed that changes in the configuration of the TCA cycle accompany cell fate transitions. During exit from pluripotency, embryonic stem cells switch from canonical to non-canonical TCA-cycle metabolism. Accordingly, blocking the non-canonical TCA cycle prevents cells from exiting pluripotency. These results establish a context-dependent alternative to the traditional TCA cycle and reveal that appropriate TCA-cycle engagement is required for changes in cell state.

Mammalian cells use diverse strategies to meet their metabolic demands. In particular, heterogeneous TCA-cycle substrate preferences and enzyme activities suggest that cells selectively engage components of the TCA cycle^{2,3}. We therefore investigated whether enzymes that are involved in the TCA cycle form discrete functional modules by analysing gene essentiality scores generated from genome-wide CRISPR screens by the DepMap project⁴, as genes participating in the same pathway exhibit similar patterns of essentiality⁵. Genes involved in core metabolic pathways were clustered on the basis of the pairwise correlation of gene essentiality scores. Of the clusters that emerged, one contained genes that are involved in glycolysis and one contained genes that are required for one-carbon metabolism, consistent with the notion that these genes comprise distinct functional modules (Extended Data Fig. 1).

Two modes of TCA-cycle metabolism

By contrast, TCA-cycle-associated genes separated into two distinct clusters, even after unbiased analysis of the top co-dependencies of all TCA-cycle genes (Extended Data Figs. 1 and 2a). Two-dimensional mapping of correlation distance demonstrated that these clusters were linked by shared co-dependency for *Dld*, a subunit that is required for both the pyruvate and oxoglutarate dehydrogenase complexes (Fig. 1a). Mapping

genes in each cluster onto the canonical TCA-cycle pathway underscored a clear division of the TCA cycle into two segments upstream and downstream of citrate (Fig. 1b), raising the question of how cells sustain citrate production if oxidative production of oxaloacetate through the TCA cycle is not tightly linked to citrate synthesis. Suggestively, enzymes involved in cytosolic citrate metabolism, including the mitochondrial citrate/malate antiporter (encoded by *Slc25a1*) and ATP citrate lyase (ACL, encoded by *Acly*), were correlated with enzymes involved in citrate production (Fig. 1a, b). The catabolism of mitochondrially derived citrate by ACL provides the cytoplasmic acetyl-CoA required for protein acetylation and lipid biosynthesis^{6,7}. The co-dependency of ACL with TCA-cycle enzymes suggests that ACL may also support cellular metabolic demands by forming a non-canonical TCA cycle that is capable of continuous oxaloacetate regeneration for citrate production.

TCA-cycle metabolism can be monitored by tracing [$U\text{-}^{13}\text{C}$]glucose, which generates citrate containing two heavy-labelled carbons (M+2-labelled citrate) following oxidative decarboxylation of glucose-derived pyruvate (Fig. 1c). Further metabolism by mitochondrial aconitase (ACO2) generates M+2-labelled TCA-cycle intermediates, whereas metabolism by ACL liberates M+2-labelled acetyl-CoA, thereby generating unlabelled oxaloacetate and downstream derivatives. Thus, a decrease in M+2 labelling of TCA-cycle intermediates downstream of

¹Cell Biology Program, Memorial Sloan Kettering Cancer Center, New York, NY, USA. ²Louis V. Gerstner Jr. Graduate School of Biomedical Sciences, New York, NY, USA. ³Weill Cornell Graduate School of Medical Sciences, Cornell University, New York, NY, USA. ⁴Human Biology Division, Fred Hutchinson Cancer Research Center, Seattle, WA, USA. ⁵Department of Epidemiology and Biostatistics, Memorial Sloan Kettering Cancer Center, New York, NY, USA. ⁶These authors contributed equally: Paige K. Arnold, Benjamin T. Jackson. ✉e-mail: finley@mskcc.org

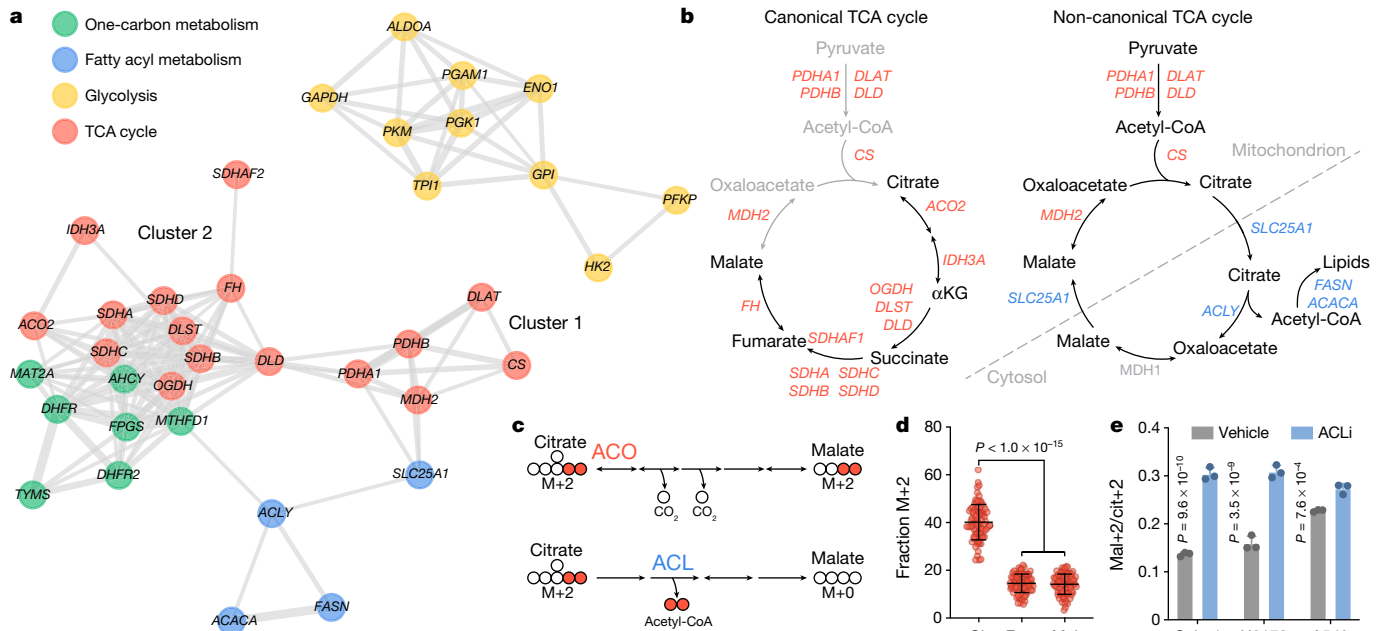


Fig. 1 | Genetic co-essentiality mapping of metabolic enzymes reveals two TCA-cycle modules. **a**, Two-dimensional network diagram representing gene essentiality score correlations between genes from the indicated pathways (Gene Ontology (GO) terms: TCA cycle, canonical glycolysis, one-carbon metabolic process and fatty-acyl-CoA metabolic process). Correlation strength is shown by the length and thickness of the connecting edge. **b**, Schematic of two TCA-cycle modules that emerge from gene clustering in **a**. Left, cluster-2 genes, associated with the pathway from citrate to malate, are annotated on the traditional TCA cycle. Right, cluster-1 genes are annotated on a non-canonical TCA cycle in which citrate is exported to the cytoplasm and cleaved by ACL to liberate acetyl-CoA and regenerate oxaloacetate, which can yield malate for mitochondrial import and oxaloacetate regeneration. Genes are coloured according to their GO term or grey (no significant correlation).

c, Schematic of the possible fates for citrate containing 2 carbons derived from [$\text{U-}^{13}\text{C}$]glucose. Top, M+2-labelled citrate metabolized by aconitase in the traditional TCA cycle generates M+2-labelled malate. Bottom, M+2-labelled citrate cleaved in the cytoplasm by ACL loses two heavy-isotope-labelled carbons, producing unlabelled four-carbon derivatives. **d**, Fractional M+2 enrichment of TCA-cycle intermediates in 82 NSCLC cell lines cultured with [$\text{U-}^{13}\text{C}$]glucose for 6 h. Data were obtained from previously published data⁸. **e**, Fractional enrichment of glucose-derived malate M+2 relative to citrate M+2 (mal+2/cit+2) in NSCLC cell lines after incubation with vehicle or 50 μM BMS-303141 (ACL inhibitor (ACLi)) for 24 h. Data are mean \pm s.d. $n = 3$ independent replicates. Significance was assessed in comparison to citrate using one-way analysis of variance (ANOVA) (**d**) or in comparison to vehicle-treated cells using two-way ANOVA (**e**) with Sidak's multiple-comparisons post-test.

citrate can partly reflect the degree to which cells engage a non-canonical TCA cycle. Many cultured cells show a disconnect between M+2 labelling of citrate and downstream metabolites, as shown in 82 non-small cell lung cancer (NSCLC) lines⁸ (Fig. 1d). To determine whether the loss of glucose label downstream of citrate is due in part to flux through ACL, we treated selected NSCLC lines with an ACL inhibitor. ACL inhibition increased the proportion of malate containing two labelled carbons while having only a small effect on the fraction of citrate M+2 (Extended Data Fig. 2b). Although glutamine anaplerosis will also contribute to a disconnect between fractional labelling of citrate and malate⁹, ACL inhibition did not uniformly affect glutamine anaplerosis, indicating that the effect of ACL on label loss downstream of citrate is not merely due to glutamine-derived label dilution (Extended Data Fig. 2c). Within an individual cell line, the degree to which malate is derived from the canonical TCA cycle can be represented as the ratio of malate M+2 relative to citrate M+2 (mal+2/cit+2). ACL inhibition increased the mal+2/cit+2 ratio in all of the cell lines, indicating that citrate metabolism by ACL contributes to the loss of glucose labelling downstream of citrate (Fig. 1e).

As an orthogonal labelling strategy, human osteosarcoma cells expressing guinea pig asparaginase¹⁰ were incubated with [$\text{U-}^{13}\text{C}$]asparagine to produce M+4-labelled citrate, which will lose labelled carbons when metabolized by the traditional TCA cycle (Extended Data Fig. 2d). Here, ACL inhibition significantly increased the ratio of cit+2/cit+4 , reflecting citrate regeneration through the oxidative TCA cycle (Extended Data Fig. 2e, f). These results are consistent with the model that citrate metabolism by ACL represents an important alternative to the canonical TCA cycle.

ES cells engage a non-canonical TCA cycle

To determine whether an ACL-mediated TCA cycle exists in non-transformed cells, we traced the fate of [$\text{U-}^{13}\text{C}$]glucose in mouse embryonic stem (ES) cells, which self-renew indefinitely when cultured with serum and leukaemia inhibitory factor (LIF). Similar to cancer cells, ES cells exhibit reduced enrichment of malate M+2 relative to citrate M+2 that is mitigated by ACL inhibition (Extended Data Fig. 3a, b). To compare the effects of ACL inhibition with disruption of the canonical TCA cycle, we generated clonal ES cell lines with genetic disruption of *Acly* or *Aco2* (Extended Data Fig. 3c, d). *Acly* disruption had no consistent effect on M+2 enrichment in citrate but consistently increased M+2 enrichment in downstream TCA-cycle metabolites, thereby elevating the mal+2/cit+2 ratio (Fig. 2a, b). By contrast, *Aco2* disruption reduced the M+2 enrichment of downstream TCA-cycle metabolites and decreased the mal+2/cit+2 ratio (Extended Data Fig. 3e). Surprisingly, despite the role of *Aco2* as a canonical TCA-cycle enzyme, *Aco2* disruption minimally affected steady-state levels of TCA-cycle metabolites (Extended Data Fig. 3f). By contrast, *Acly* mutation substantially altered levels of TCA-cycle metabolites that are associated with cytosolic citrate processing (citrate, malate, aspartate and fumarate), but not canonical TCA-cycle metabolism (succinate, α -ketoglutarate) (Fig. 2c).

To test the hypothesis that a portion of the TCA cycle flows through ACL, we directly tested whether ACL mediates citrate recycling. Cytosolic processing of citrate to malate requires hydride donation from NADH, which can be traced by culturing cells with [$4\text{-}^2\text{H}$]glucose to label up to half of cytosolic NADH pools¹¹ (Fig. 2d). *Acly* mutation did

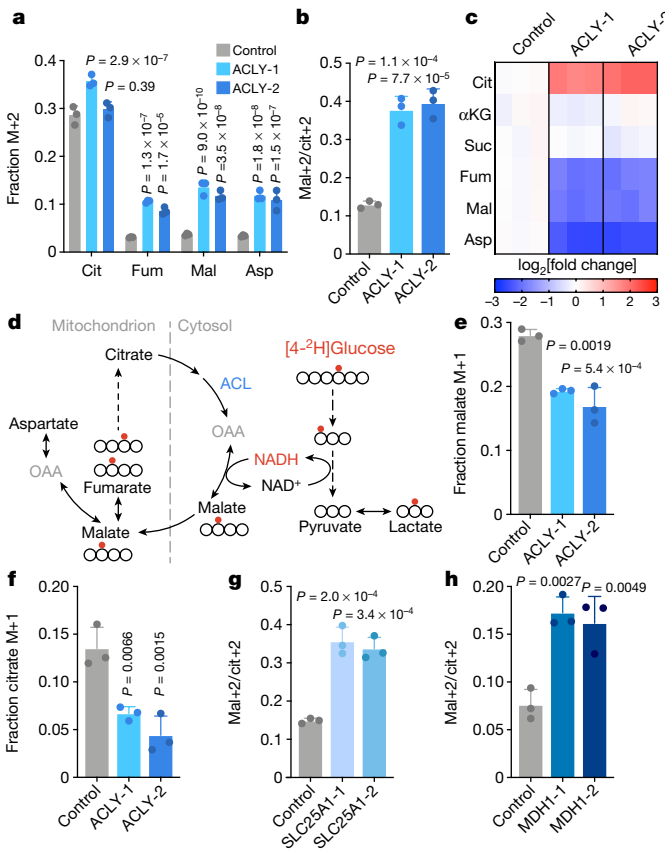


Fig. 2 | ACL loss disrupts TCA-cycle metabolism in ES cells. **a, b**, Fractional M+2 enrichment of citrate (Cit), fumarate (Fum), malate (Mal) and aspartate (Asp) (**a**) or malate M+2 relative to citrate M+2 (mal+2/cit+2) (**b**) in control and *Acly*-edited (ACLY-1 and ACLY-2) mouse ES cells cultured in medium containing [$U\text{-}^{13}\text{C}$]glucose. **c**, Steady-state levels of TCA-cycle metabolites in *Acly*-edited mouse ES cells. Levels are represented as the \log_2 -transformed fold change relative to the control cells. αKG , α -ketoglutarate; Suc, succinate. **d**, Schematic of deuterium label transfer from [4- ^2H]glucose first onto NADH during glycolysis and subsequently onto either malate or lactate in the cytoplasm through MDH1 or LDH activity, respectively. After mitochondrial import, deuterium-labelled malate can be converted to fumarate. The symmetry of fumarate allows the deuterium label to be scrambled, enabling the generation of deuterium-labelled citrate. OAA, oxaloacetate. **e, f**, Fractional M+1 enrichment of malate (**e**) or citrate (**f**) in control and *Acly*-edited ES cells cultured in medium containing [4- ^2H]glucose. **g, h**, The mal+2/cit+2 ratio derived from [$U\text{-}^{13}\text{C}$]glucose in control and *Slc25a1*-edited (**g**) or *Mdh1*-edited (**h**) ES cells. Data are mean \pm s.d. $n = 3$ independent replicates. Significance was assessed using two-way ANOVA (**a**) or one-way ANOVA (**b** and **e–h**) with Sidak's multiple-comparisons post-test relative to the controls.

not affect NADH labelling from [4- ^2H]glucose: both control and edited cells exhibit similar fractional enrichment of NADH and lactate, which becomes labelled when lactate dehydrogenase reduces cytosolic pyruvate (Extended Data Fig. 3g, h). However, *Acly*-edited clones did display significantly lower M+1 enrichment of malate, indicating that wild-type cells generate a portion of malate by reducing ACL-derived cytosolic oxaloacetate (Fig. 2e). Importantly, *Acly* mutation more than halved the fraction of labelled citrate, suggesting that cytosolic malate is indeed recycled back into the mitochondria for citrate regeneration, and that this process is impaired in the absence of ACL (Fig. 2f and Extended Data Fig. 3i–k). Consistent with impaired transfer of cytosolic reducing equivalents to the mitochondria, *Acly* mutation increased the cytosolic NADH/NAD $^+$ ratio, measured as the ratio of lactate to pyruvate¹², and decreased mitochondrial oxygen consumption (Extended Data Fig. 3l, m).

To further test whether SLC25A1, ACL and MDH1 form a non-canonical TCA cycle, we generated clonal ES cell lines deficient for SLC25A1 and MDH1 (Extended Data Fig. 4a, b). Deuterated glucose tracing revealed that, like ACL, both SLC25A1 and MDH1 were required for citrate regeneration from cytosolic oxaloacetate (Extended Data Fig. 4c, d). Accordingly, *Slc25a1*- and *Mdh1*-edited cells exhibited [$U\text{-}^{13}\text{C}$]glucose labelling patterns that were consistent with reduced non-canonical TCA-cycle activity, including increased enrichment of M+2 isotopologues in TCA-cycle metabolites downstream of citrate and an elevated mal+2/cit+2 ratio (Fig. 2g, h and Extended Data Fig. 4e, f). Furthermore, *Slc25a1* and *Mdh1* mutation, like *Acly* mutation, reduced malate and fumarate pools (Extended Data Fig. 4g). SLC25A1 loss also reduced aspartate pools, but MDH1 loss did not, consistent with its role in the malate–aspartate shuttle that consumes cytosolic aspartate¹³. These data demonstrate that SLC25A1, ACL and MDH1 coordinate a cross-compartment cycle of citrate metabolism.

TCA-cycle choice is cell-state dependent

As Krebs originally elucidated the canonical TCA cycle in pigeon breast muscle¹⁴, we assessed TCA-cycle choice in C2C12 myoblasts and differentiated myotubes. Compared with myoblasts, myotubes exhibited increased incorporation of glucose-derived carbons into TCA-cycle intermediates and a mal+2/cit+2 ratio of greater than fivefold higher than proliferating myoblasts (Fig. 3a and Extended Data Fig. 5a, b). Consistent with switching from the non-canonical to canonical TCA cycle, [4- ^2H]glucose tracing revealed a diminished production of malate, fumarate and citrate from cytosolic oxaloacetate in myotubes compared with in myoblasts (Extended Data Fig. 5c). To further assess TCA-cycle engagement, we engineered cells to express doxycycline-inducible short hairpin RNAs (shRNAs) targeting *Acly* or *Aco2* (Extended Data Fig. 5d). ACL inhibition significantly increased the mal+2/cit+2 ratio in myoblasts, but not myotubes (Extended Data Fig. 5e–h). By contrast, although ACO2 inhibition decreased the mal+2/cit+2 ratio in myoblasts, this effect was greater in myotubes, consistent with canonical TCA-cycle engagement after differentiation (Extended Data Fig. 5e–h). As in ES cells, ACL inhibition significantly increased citrate pools and decreased the levels of fumarate, malate and aspartate, and this effect was stronger in myoblasts compared with in myotubes (Fig. 3b). By contrast, ACO2 inhibition had little effect on the levels of TCA-cycle metabolites in myoblasts and, surprisingly, tended to increase metabolite levels in myotubes, indicating that ACO2 loss causes greater metabolic disruption in myotubes compared with in myoblasts (Fig. 3b). Collectively, these results indicate that the degree to which cells use the canonical TCA cycle is at least partially determined by cell state.

To identify potential drivers of TCA-cycle choice, we compared gene expression with TCA-cycle activity in NSCLC lines. TCA-cycle genes were highly enriched among genes that were positively correlated with the mal+2/cit+2 ratio (Extended Data Fig. 6a). Similarly, myogenic differentiation significantly induced most TCA-cycle genes, many of which are targets of the myogenic transcription factor MYOD¹⁵ (Fig. 3c). As all of the subunits of the pyruvate dehydrogenase complex (PDHC), which initiates carbon entry into the TCA cycle, were upregulated after myogenic differentiation, we tested whether modulating pyruvate entry into the TCA cycle affected the TCA-cycle choice. Both myoblasts and ES cells that were treated with dichloroacetate to potentiate PDHC activity¹⁶ increased the incorporation of glucose-derived carbons not only into citrate but also into downstream metabolites, thereby increasing the mal+2/cit+2 ratio consistent with enhanced canonical TCA-cycle activity (Fig. 3d, e and Extended Data Fig. 6b, c). Reciprocally, pharmacological inhibition of the mitochondrial pyruvate carrier reduced incorporation of glucose-derived carbons into TCA-cycle metabolites and repressed the mal+2/cit+2 ratio (Fig. 3d, e and Extended Data Fig. 6b, c). Thus, TCA-cycle choice is determined in part by the amount of pyruvate captured for oxidation by PDHC.

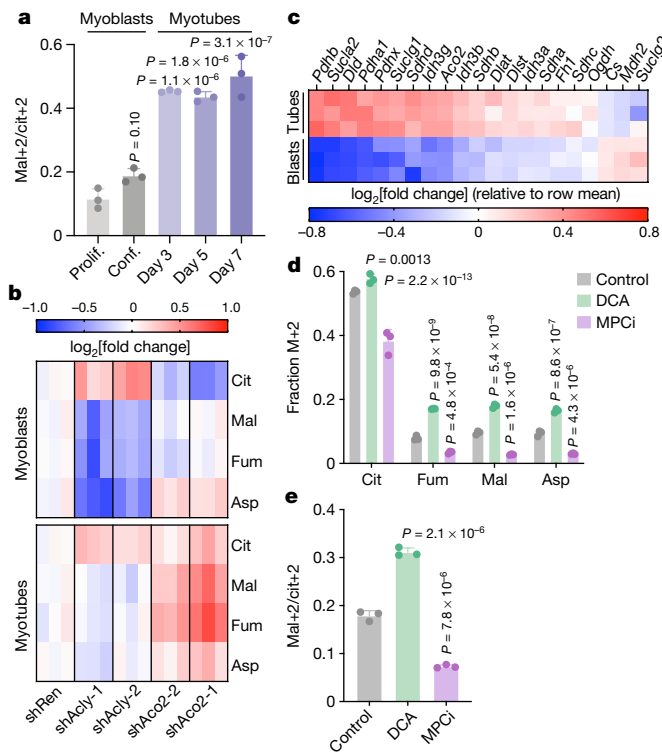


Fig. 3 | Engagement of the non-canonical TCA cycle is cell-state dependent. **a**, Fractional enrichment of malate M+2 relative to citrate M+2 ($\text{mal}+2/\text{cit}+2$) derived from [^{13}C]glucose in proliferating (prolif.) and confluent (conf.) myoblasts and myotubes differentiated for 3, 5 or 7 days. **b**, Steady-state levels of citrate, fumurate, malate and aspartate, expressed as the \log_2 -transformed fold change relative to shRenilla, in myoblasts (top) and myotubes (bottom). Myoblasts and myotubes expressing doxycycline-inducible shRNAs targeting *Acly* (shAcly-1 and shAcly-2), *Aco2* (shAco2-1 and shAco2-2) or *Renilla* luciferase (shRen, used as a control) were cultured on doxycycline for two or four days, respectively, to induce shRNA expression. **c**, RNA-seq analysis of TCA-cycle-associated genes in myoblasts (blasts) and myotubes (tubes) that were differentiated for 5 days. Levels are represented as the \log_2 -transformed fold change relative to the row mean. $n = 3$ independently derived samples. **d, e**, Fractional M+2 enrichment (**d**) or the $\text{mal}+2/\text{cit}+2$ ratio (**e**) derived from [^{13}C]glucose in myoblasts after treatment with vehicle (control), 5 mM dichloroacetate (DCA) or 10 μM UK-5099 (MPCi) for 24 h. Data are mean \pm s.d. $n = 3$ independent replicates. Significance was assessed in comparison to proliferating myoblasts (**a**) or vehicle treatment (**d** and **e**) using one-way ANOVA (**a** and **e**) or two-way ANOVA (**d**) with Sidak's multiple-comparisons post-test.

TCA-cycle switch after pluripotency exit

We next examined whether changes in TCA-cycle configuration are required for changes in cell state. ES cells cultured with LIF and inhibitors against GSK3 β and MEK (2i) represent the naive ground state of pluripotency reminiscent of the pre-implantation epiblast; withdrawal of these factors (-2i/LIF) enables cells to exit the naive pluripotent state and gain differentiation competence¹⁷ (Extended Data Fig. 7a–c). Loss of naive pluripotency triggers major changes in TCA-cycle dynamics: cells induced to exit naive pluripotency decrease incorporation of glucose-derived carbon while increasing incorporation of glutamine-derived carbon (Extended Data Fig. 7d, e), consistent with our previous report demonstrating enhanced glutamine dependence in more committed ES cells¹⁸. The high $\text{mal}+2/\text{cit}+2$ ratio of naive ES cells is progressively reduced during exit from naive pluripotency alongside a concomitant increase in citrate production from cytosolic intermediates (Fig. 4a, b and Extended Data Fig. 7f). This metabolic shift was not due to changes in the culture medium: ES cells cultured serum-free in 2i/LIF

also repressed glucose utilization and had a decreased $\text{mal}+2/\text{cit}+2$ ratio after 2i/LIF withdrawal, despite continuous culture in the same medium formulation (Extended Data Fig. 7g–i). Furthermore, cells deficient for *Tcf3/Tcf7l1*, a repressor of the naive pluripotency gene network¹⁹, exhibited dampened metabolic reprogramming corresponding to a delayed exit from naive pluripotency (Extended Data Fig. 7j–m).

Together, these results indicate that ES cells switch from canonical to non-canonical TCA-cycle activity as they dismantle naive pluripotency. Accordingly, metabolic rewiring during exit from pluripotency required *ACL–Acly*-edited clones maintained higher incorporation of glucose-derived carbons and lower incorporation of glutamine-derived carbons compared with their control counterparts grown in -2i/LIF conditions (Extended Data Fig. 8a, b). *ACL* loss did not affect the $\text{mal}+2/\text{cit}+2$ ratio or steady-state levels of TCA-cycle metabolites in naive ES cells, but doubled the $\text{mal}+2/\text{cit}+2$ ratio and triggered up to sevenfold changes in TCA-cycle metabolite levels in cells grown under -2i/LIF conditions (Extended Data Fig. 8c–f). As a consequence, *ACL* was required for inducing large changes in TCA-cycle metabolites and maintaining viability specifically after exit from naive pluripotency (Fig. 4c and Extended Data Fig. 8g). Impaired viability was not due simply to deficient cytosolic acetyl-CoA after *ACL* loss: exogenous acetate restored histone acetylation and supported de novo lipid synthesis—processes that require cytosolic acetyl-CoA⁷—but minimally rescued viability (Extended Data Fig. 8h–k). Thus, after exit from naive pluripotency, cells rely on the non-canonical TCA cycle to maintain TCA-cycle intermediates and cell viability.

Exit from pluripotency requires *ACL*

We therefore tested whether exit from naive pluripotency requires *ACL*. Using ES cells containing a reporter of naive pluripotency (*Rex1::GFPd2*)²⁰, we found that the expected reporter downregulation after 2i/LIF withdrawal¹⁷ was almost completely prevented by *ACL* inhibition (Fig. 4d and Extended Data Fig. 8l). Similarly, following 2i/LIF withdrawal, *Acly*-edited clones demonstrated increased expression of the naive pluripotency genes *Nanog*, *Esrrb* and *Rex1*, impaired induction of the differentiation marker *Sox1* and an enhanced ability to form alkaline-phosphatase-positive colonies when reseeded into medium containing 2i/LIF (Fig. 4e and Extended Data Fig. 8m, n). None of these phenotypes were reversed by exogenous acetate, which tended to increase colony formation (Extended Data Fig. 8o–q), consistent with reports that acetate promotes ES cell self-renewal²¹. These results demonstrate that *ACL* loss selectively impairs the metabolism and viability of cells during 2i/LIF withdrawal, independent of cytosolic acetyl-CoA.

Like *ACL*, neither *SLC25A1* nor *MDH1* was required for the viability of naive pluripotent ES cells (Extended Data Fig. 9a). Moreover, like *ACL*, the loss of *SLC25A1* specifically impaired the viability of cells under -2i/LIF conditions, but the loss of *MDH1* did not (Extended Data Fig. 9b). Notably, although *ACL*, *SLC25A1* and *MDH1* were all required to sustain the TCA-cycle metabolites fumarate and malate during exit from naive pluripotency, only *SLC25A1* and *ACL* were required to maintain aspartate pools (Extended Data Fig. 9c). Aspartate, which contributes to protein and nucleotide biosynthesis, is a critical output of the TCA cycle in proliferating cells^{13,22}. Consistent with this, when induced to exit naive pluripotency, both *Acly*- and *Slc25a1*-edited cells, but not *Mdh1*-edited cells, had impaired protein synthesis and reduced proliferation (Extended Data Fig. 9d–g). Accordingly, while *Acly*- and *Slc25a1*-edited cells preserved naive pluripotency gene signatures, this effect was blunted in *Mdh1*-edited cells (Extended Data Fig. 9h, i). Together, these results demonstrate that *SLC25A1*, *ACL* and *MDH1* establish metabolic identity as cells exit the naive pluripotent state, and cells that are unable to activate *ACL*-dependent non-canonical TCA-cycle metabolism exhibit compromised viability.

To further test the model that appropriate TCA-cycle engagement enables establishment of cell identity, we tested whether efficient induction of the naive, ground state of pluripotency requires canonical TCA-cycle metabolism. *Aco2* disruption did not affect proliferation

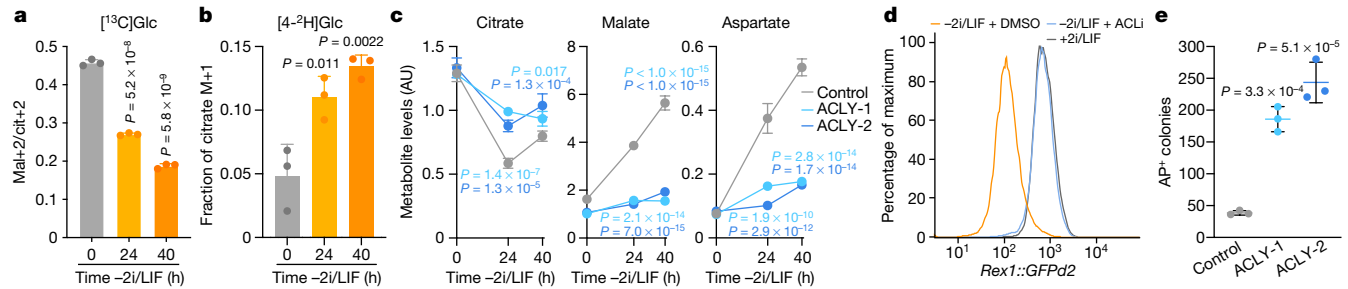


Fig. 4 | Exit from naive pluripotency requires engagement of the non-canonical TCA cycle. **a, b**, Fractional enrichment of malate M+2 relative to citrate M+2 (mal+2/cit+2) derived from [^{13}C]glucose (Glc) (**a**) or citrate M+1 derived from [^{4-2}H]glucose (**b**) in ES cells subjected to 2i/LIF withdrawal for the indicated times. **c**, Steady-state levels of metabolites in control and *Acy*-edited ES cells grown under -2i/LIF conditions for the indicated times. **d**, GFP intensity encoded by the *Rex1::GFPd2* reporter in ES cells subjected to 2i/LIF withdrawal for 40 h in the presence of vehicle or 50 μM MBMS-303141 (ACLi). Naive ES cells (+2i/LIF) were included as a control. **e**, Quantification of alkaline phosphatase positive (AP⁺) colonies representing control and *Acy*-edited ES cells that did

not exit the naive pluripotent state. 2i-adapted ES cells subjected to 2i/LIF withdrawal for 40 h were reseeded at clonal density into medium containing 2i/LIF. One histogram representative of four replicates with similar results shown in **d**. For all other panels, data are mean \pm s.d. $n = 3$ independent replicates. Significance was assessed using two-way ANOVA with Sidak's multiple-comparisons post-test relative to control cells at each timepoint with *P* values coloured according to comparison (**c**), or by one-way ANOVA in comparison to 0 h (**a** and **b**) or control cells (**e**) with Sidak's multiple-comparisons post-test.

in serum/LIF-cultured ES cells, which exhibit non-canonical TCA-cycle activity (Extended Data Fig. 10a). Supplementing the cells with 2i to initiate conversion to naive pluripotency slowed the proliferation of *Aco2*-edited clones and delayed the induction of naive pluripotency markers (Extended Data Fig. 10b, c). Collectively, these results underscore the role of TCA-cycle configuration in facilitating cell state transitions.

Discussion

Here we identified a non-canonical TCA cycle that is active in both normal and transformed cells. The possibility of a similar citrate–malate shuttle has been proposed but has never been demonstrated^{6,23,24}. By combining isotope tracing with genetic manipulation of ACL, SLC25A1 and MDH1, we provide direct evidence that the proposed citrate–malate shuttle indeed represents a bona fide cycle with differential activity across mammalian cell states. Potential advantages of non-canonical TCA-cycle engagement include retaining, rather than combusting, reduced carbon and regenerating cytosolic NAD⁺ required to sustain glycolysis. By circumventing several steps of the mitochondrial TCA cycle, the non-canonical TCA cycle maintains oxaloacetate regeneration while minimizing mitochondrial NADH production, which may restrain cell proliferation²⁵. Notably, in contrast to their in vitro counterparts, cancer cells growing in vivo exhibit little loss of glucose label between citrate and malate^{26,27}, suggesting that differential TCA-cycle engagement contributes to the discrepancy between in vitro and in vivo metabolic phenotypes. Consistent with this, pancreatic cancer cells are more reliant on *Acy* in vitro and more dependent upon *Aco2* in vivo²⁸. Collectively, these studies underscore the diversity of metabolic strategies that support cellular bioenergetics and reveal that TCA-cycle behaviour is dynamic and entwined with cell state.

Online content

Any methods, additional references, Nature Research reporting summaries, source data, extended data, supplementary information, acknowledgements, peer review information; details of author contributions and competing interests; and statements of data and code availability are available at <https://doi.org/10.1038/s41586-022-04475-w>.

- DeBerardinis, R. J. & Chandel, N. S. Fundamentals of cancer metabolism. *Sci. Adv.* **2**, e1600200 (2016).
- Kim, J. & DeBerardinis, R. J. Mechanisms and implications of metabolic heterogeneity in cancer. *Cell Metab.* **30**, 434–446 (2019).
- Muir, A., Danai, L. V. & Vander Heiden, M. G. Microenvironmental regulation of cancer cell metabolism: implications for experimental design and translational studies. *Dis. Model. Mech.* **11**, dmm035758 (2018).
- Tsherniak, A. et al. Defining a cancer dependency map. *Cell* **170**, 564–576 (2017).
- Wainberg, M. et al. A genome-wide atlas of co-essential modules assigns function to uncharacterized genes. *Nat. Genet.* **53**, 638–649 (2021).
- Hatzivassiliou, G. et al. ATP citrate lyase inhibition can suppress tumor cell growth. *Cancer Cell* **8**, 311–321 (2005).
- Zhao, S. et al. ATP-citrate lyase controls a glucose-to-acetate metabolic switch. *Cell Rep.* **17**, 1037–1052 (2016).
- Chen, P. H. et al. Metabolic diversity in human non-small cell lung cancer cells. *Mol. Cell* **76**, 838–851 (2019).
- Alves, T. C. et al. Integrated, step-wise, mass-isotopomeric flux analysis of the TCA cycle. *Cell Metab.* **22**, 936–947 (2015).
- Sullivan, L. B. et al. Aspartate is an endogenous metabolic limitation for tumour growth. *Nat. Cell Biol.* **20**, 782–788 (2018).
- Lewis, C. A. et al. Tracing compartmentalized NADPH metabolism in the cytosol and mitochondria of mammalian cells. *Mol. Cell* **55**, 253–263 (2014).
- Williamson, D. H., Lund, P. & Krebs, H. A. The redox state of free nicotinamide-adenine dinucleotide in the cytoplasm and mitochondria of rat liver. *Biochem. J.* **103**, 514–527 (1967).
- Birsoy, K. et al. An essential role of the mitochondrial electron transport chain in cell proliferation is to enable aspartate synthesis. *Cell* **162**, 540–551 (2015).
- Krebs, H. A. & Eggleston, L. V. The oxidation of pyruvate in pigeon breast muscle. *Biochem. J.* **34**, 442–459 (1940).
- Shintaku, J. et al. MyoD regulates skeletal muscle oxidative metabolism cooperatively with alternative NF- κ B. *Cell Rep.* **17**, 514–526 (2016).
- Stacpoole, P. W. The pharmacology of dichloroacetate. *Metabolism* **38**, 1124–1144 (1989).
- Kalkan, T. et al. Tracking the embryonic stem cell transition from ground state pluripotency. *Development* **144**, 1221–1234 (2017).
- Vardhana, S. A. et al. Glutamine independence is a selectable feature of pluripotent stem cells. *Nat. Metab.* **1**, 676–687 (2019).
- Pereira, L., Yi, F. & Merrill, B. J. Repression of Nanog gene transcription by Tcf3 limits embryonic stem cell self-renewal. *Mol. Cell. Biol.* **26**, 7479–7491 (2006).
- Wray, J. et al. Inhibition of glycogen synthase kinase-3 alleviates Tcf3 repression of the pluripotency network and increases embryonic stem cell resistance to differentiation. *Nat. Cell Biol.* **13**, 838–845 (2011).
- Moussaieff, A. et al. Glycolysis-mediated changes in acetyl-CoA and histone acetylation control the early differentiation of embryonic stem cells. *Cell Metab.* **21**, 392–402 (2015).
- Sullivan, L. B. et al. Supporting aspartate biosynthesis is an essential function of respiration in proliferating cells. *Cell* **162**, 552–563 (2015).
- Borst, P. The malate-aspartate shuttle (Borst cycle): how it started and developed into a major metabolic pathway. *IUBMB Life* **72**, 2241–2259 (2020).
- Assmann, N. et al. Srebp-controlled glucose metabolism is essential for NK cell functional responses. *Nat. Immunol.* **18**, 1197–1206 (2017).
- Luengo, A. et al. Increased demand for NAD⁺ relative to ATP drives aerobic glycolysis. *Mol. Cell* **81**, 691–707 (2020).
- Davidson, S. M. et al. Environment impacts the metabolic dependencies of Ras-driven non-small cell lung cancer. *Cell Metab.* **23**, 517–528 (2016).
- Marín-Valencia, I. et al. Analysis of tumor metabolism reveals mitochondrial glucose oxidation in genetically diverse human glioblastomas in the mouse brain in vivo. *Cell Metab.* **15**, 827–837 (2012).
- Zhu, X. G. et al. Functional genomics in vivo reveal metabolic dependencies of pancreatic cancer cells. *Cell Metab.* **33**, 211–221 (2021).

Publisher's note Springer Nature remains neutral with regard to jurisdictional claims in published maps and institutional affiliations.

© The Author(s), under exclusive licence to Springer Nature Limited 2022

Methods

Metabolic co-essentiality analysis and network modelling

To obtain metabolic gene essentiality scores, we analysed CERES gene dependency values from the DepMap Portal Project Achilles^{29,30} 20Q2 release in which 18,119 genes were perturbed by genome-wide loss of function CRISPR screens in 769 human cancer cell lines. We used two gene lists to perform our analysis. To focus on an unbiased set of metabolic genes corresponding to well-defined metabolic pathways, we created a gene set of 122 genes derived from four GO terms^{31,32}: tricarboxylic acid cycle (GO:0006099), canonical glycolysis (GO:0061621), 1-carbon metabolic process (GO:0006730) and fatty-acyl-CoA metabolic process (GO:0035337). To focus more specifically on the TCA cycle, we used a list of 27 core TCA-cycle genes and then identified the top 10 correlates of these genes using Pearson correlation coefficients from DepMap gene essentiality scores above a minimum threshold ($r > 0.25$). Next, we identified the top 5 correlates of this expanded list again above a minimum threshold ($r > 0.25$), resulting in a list of 115 TCA-cycle associated genes.

To examine genetic co-dependency in these gene lists, Pearson correlation coefficients were calculated between metabolic gene essentiality scores across the 769 human cancer cell lines surveyed to generate a correlation matrix heat map of codependent gene modules. To create the heat map, the correlations were hierarchically clustered with the UPGMA algorithm using the `scipy.cluster.hierarchy.linkage` function from the SciPy Python package³³, with the method argument set to ‘average’. The heat map was graphed using the Seaborn Python package (<https://seaborn.pydata.org/citing.html>). To visualize codependent gene modules as a network diagram, we used the Python package NetworkX (<http://networkx.org>). Genes with no correlation partners or with low correlation scores ($r < 0.25$) were filtered out, and spring model layouts were generated using the method ‘neato’ from the Python package PyGraphviz (<http://pygraphviz.github.io>). Graph edges were weighted according to the strength of pairwise gene correlations and the final network diagram was created using the NetworkX draw function. Gene clusters with less than three members were removed.

Gene expression correlation

NSCLC cell line isotope tracing data were obtained from previously published data⁸. Gene expression data were obtained from the DepMap Cancer Cell Line Encyclopedia³⁴. For the 68 cell lines present in both datasets, expression of each gene was correlated with the fractional enrichment of malate M+2 relative to citrate M+2 (mal+2/cit+2) derived from [$\text{U-}^{13}\text{C}$]glucose. Genes were ranked on the basis of correlation with mal+2/cit+2, and gene set enrichment analysis³⁵ of the gene set KEGG citric acid (TCA) cycle-associated genes (KEGG_CITRATE_CYCLE_TCA_CYCLE; M3985) was performed using GSEAPreranked version 4 with the default parameters. Data were exported and graphed in GraphPad Prism v.9.

Cell culture

Mouse ES cells were previously generated from C57BL/6 × 129S4/SvJae F₁ male embryos³⁶. *Rex1::GFPd2* ES cells²⁰ were a gift from A. Smith. All other cell lines were obtained from ATCC. ES cells were maintained on gelatin-coated plates in the following media: serum/LIF, serum/LIF+2i or 2i/LIF. Serum/LIF medium contained knockout DMEM (10829018; Thermo Fisher Scientific) supplemented with 10% fetal bovine serum (FBS; Gemini), 0.1 mM 2-mercaptoethanol, 2 mM L-glutamine and 1,000 U ml⁻¹ LIF (Gemini). To generate serum/LIF+2i maintenance medium, serum/LIF medium was supplemented with 3 µM CHIR99021 (Stemgent) and 1 µM PD0325901 (Stemgent) (2i). 2i/LIF medium contained a 1:1 mix of DMEM/F-12 (11320033; Gibco) and Neurobasal medium (21103049; Gibco) including N-2 supplement (17502048; Gibco), B-27 supplement (17504044; Gibco), 2-mercaptoethanol, 2 mM L-glutamine, LIF and 2i. To generate ES cells in the naive ground state

of pluripotency, serum/LIF-cultured ES cells were adapted for three passages to serum/LIF+2i medium or 2i/LIF medium. Adapted cells were used for a maximum of nine passages.

For exit from naive pluripotency, serum/LIF+2i-cultured ES cells were seeded at least 24 h before washing with PBS and changing into medium containing a 1:1 mix of glutamine-free DMEM (11960051; Gibco) and Neurobasal medium including N-2 supplement, B-27 supplement, 2-mercaptoethanol and 2 mM L-glutamine at the indicated time before collection (24 or 40 h). 2i/LIF-cultured ES cells were seeded at least 24 h before being washed with PBS and changed into serum-free maintenance medium without 2i or LIF at the indicated time before collection (12, 24 or 40 h). Unless otherwise noted, cells were adapted to serum/LIF+2i culture before exit from naive pluripotency.

C2C12 cells were maintained at subconfluence as myoblasts unless otherwise noted. All myoblast experiments were performed in high-glucose DMEM supplemented with 10% FBS and 4 mM L-glutamine. For differentiation into myotubes, C2C12 cells were grown to 100% confluence for 3 days and then washed with PBS and changed into differentiation medium composed of high-glucose DMEM supplemented with 2% horse serum (26050070; Gibco), 4 mM L-glutamine and 100× insulin–transferrin–selenium–ethanolamine (ITS-X; 51500056; Gibco) for the indicated length of time (3, 5 or 7 days). Differentiation medium was refreshed every day. For NSCLC cell line studies, the H2170, A549 and Calu-1 cell lines were thawed and passaged in RPMI-1640 supplemented with 10% FBS before being transitioned to high-glucose DMEM supplemented with 10% FBS and 4 mM L-glutamine for several passages before the experiments. 143B cells were maintained in high-glucose DMEM supplemented with sodium pyruvate, 10% FBS and penicillin–streptomycin. Cell lines treated with inhibitors were cultured as described above but the medium was supplemented with DMSO, 50 µM BMS-303141 (SML0784; Sigma-Aldrich), 5 mM dichloroacetate (3447795; Sigma-Aldrich) or 10 µM UK-5099 (4186; Tocris) for 24 h before collection or for the duration of the exit from pluripotency. Cell lines were not externally authenticated. All cells routinely tested negative for mycoplasma.

Generation of clonal ES cell lines

Single guide RNA (sgRNA) sequences targeting *Acly*, *Aco2*, *Slc25a1*, *Mdh1* or a control, non-genic region on mouse chromosome 8³⁷ were cloned into the pSpCas9(BB)-2A-GFP plasmid (PX458, Addgene plasmid number 48138), as previously described³⁸. A list of sgRNA sequences is provided in Supplementary Table 2. ES cells (4×10^5 per condition) were electroporated using the 4D-Nucleofector (Amaxa, Lonza) system with 5 µg PX458 plasmid encoding Cas9, EGFP and sgRNA sequences. After electroporation, cells were plated onto a layer of mitotically inactivated feeder mouse embryonic fibroblasts (MEFs). After 48 h, cells were dissociated with Accutase (Invitrogen) and sorted using the BD FACSAria III sorter (BD Biosciences) to enrich for GFP-positive cells. Approximately 10,000 fluorescence-activated cell sorting (FACS)-sorted GFP-positive cells per experimental condition were immediately reseeded onto 10 cm plates (on feeder MEFs) to enable clonal growth. After 7 days, individual clones were picked and expanded (initially on feeder MEFs, then on gelatin-coated tissue culture plates) and loss of target gene expression was validated by immunoblotting (see below).

Generation of *Tcf7l1*-edited ES cell lines

*Cas9*cDNA from a lentiCas9-Blast plasmid (Addgene plasmid number 52962) was cloned into Piggybac (pCAGGS-IRES-Neo, a gift from H. Niwa). ES cells were transfected with Piggybac plus transposase (pBase) at a ratio of 3:1 using Fugene HD (E2691; Promega). After selection with G418 (300 µg ml⁻¹, 10131-035; Gibco), cells were plated on feeder MEFs at a single-cell density to generate clonal Cas9⁺ ES cell lines.

sgRNA sequences targeting *Tcf7l1*(ref.³⁹) or a non-genic region on mouse chromosome 8 were cloned into the pUSEPB plasmid⁴⁰ (gift from S. Lowe) as previously described³⁸. A list of sgRNA sequences

is provided in Supplementary Table 2. Lentivirus was generated by the co-transfection of sgRNA vectors with the packaging plasmids psPAX2 and pMD2.G (Addgene) into HEK293T cells. Virus-containing supernatant was cleared of cellular debris by 0.45 µm filtration and was concentrated using Lenti-X (631231; Takara). Cas9-ES cells were exposed to concentrated viral supernatant with 6 µg ml⁻¹ polybrene for 24 h before being washed, grown for 24 h in fresh medium and selected for using antibiotics. Cells were expanded and loss of target gene expression was validated by immunoblotting (see below).

sgRNA editing analysis

For clonal ES cell lines, genomic DNA was extracted (Qiagen) and amplification of edited regions was performed from 50 ng of genomic DNA using Platinum Taq DNA Polymerase (Invitrogen) according to the manufacturer's instructions. A list of sequencing primers is provided in Supplementary Table 3. Primers were optimized to produce an amplicon of between 200 and 280 bp long and containing the edited locus within the first 100 bp (from either the 5'-end or 3'-end). The PCR products were column purified (Qiagen), and the detection of CRISPR variants from NGS reads (CRISPR sequencing) was performed by the CCIB DNA Core Facility at Massachusetts General Hospital. In brief, Illumina-compatible adapters with unique barcodes were ligated onto each sample during library construction. Libraries were pooled in equimolar concentrations for multiplexed sequencing on the Illumina MiSeq platform with 2 × 150 run parameters. After completing the NGS run, data were demultiplexed and subsequently entered into an automated de novo assembly pipeline, UltraCycler v.1.0 (B. Seed and H. Wang, https://dnacore.mgh.harvard.edu/new-cgi-bin/site/pages/crispr_sequencing_pages/crispr_sequencing_algorithm.jsp). Sequenced amplicons produced for each clonal ES cell line are listed and annotated in Supplementary Table 3.

Lentiviral production and infection

Renilla luciferase-, *Acly*- and *Aco2*-targeting shRNAs were introduced into C2C12 cells to enable doxycycline-inducible expression using lentiviral LT3GEPiR⁴¹ (the shRNA sequences are provided in Supplementary Table 2). The lentivirus was generated by the co-transfection of shRNA-expressing viral vectors with the packaging plasmids psPAX2 and pMD2.G (Addgene) into HEK293T cells. Virus-containing supernatants were cleared of cellular debris by 0.45 µm filtration and mixed with 8 µg ml⁻¹ polybrene. C2C12 cells were exposed to viral supernatants for two 24 h periods before being passaged and grown for 24 h in fresh medium and then subjected to antibiotic selection with 1 µg ml⁻¹ puromycin. Cells were maintained under antibiotic selection until all cells on an uninfected control well were eliminated.

Viability assays

Serum/LIF+2i-adapted ES cells were seeded at a density of 24,000 cells per well of a 24-well plate in triplicate or quadruplicate. Then, 24 h later, the cells were washed with PBS and changed into either fresh serum/LIF+2i medium or medium containing a 1:1 mix of glutamine-free DMEM and Neurobasal medium including N-2 supplement, B-27 supplement, 2-mercaptoethanol and 2 mM L-glutamine for 40 h. The cells were evaluated for propidium iodide on the LSRFortessa flow cytometer using FACSDiva software v.8.0 (BD Biosciences). Analysis of propidium iodide exclusion was performed using FCS Express v.7.05 or FlowJo v.10.8.0.

Growth curves

ES cells were seeded at a density of 40,000 cells per well of a 12-well plate. The next day, three wells of each line were counted to determine the starting cell number. The remaining cells were washed with PBS and either changed to medium containing serum/LIF+2i or induced to exit from naive pluripotency as indicated above. Cells were counted 40 h later using a Beckman Coulter Multisizer 4e with a cell volume gate of

400–10,000 fl. Cell counts were normalized to starting cell number. All curves were performed at least two independent times.

Naive pluripotency conversion growth curve

ES cells were seeded in standard culture medium (serum/LIF) in six-well plates; then, 48 h later, cells were counted to establish a baseline measurement of proliferation for each line under serum/LIF culturing conditions. After this count, ES cells were seeded into serum/LIF+2i maintenance medium and passaged and counted every 48 h for 6 days (three passages). Cumulative population doublings were assessed by summing population doublings measured at each passage. Cells were counted using a Beckman Coulter Multisizer 4e with a cell volume gate of 400–10,000 fl.

OP-puro assay

All cells were washed with PBS and changed into fresh medium 60 min before collection. For cycloheximide control samples, 10 µg ml⁻¹ cycloheximide was added to wells at this time. At 30 min before collection, 20 µM O-propargyl-puromycin (OP-puro, HY-15680; MedChemExpress) was added to cells. Cells were collected and stained with fixable viability dye (65-0863-14; Thermo Fisher Scientific), followed by fixation with 4% PFA in PBS and permeabilization with 0.25% Triton-X-100. Fixed and permeabilized cells were stained using the Click-iT Plus Alexa Fluor 647 Picolyl Azide Toolkit (C10643; Thermo Fisher Scientific) and AZDye 647 Picolyl Azide (1300-1; Click Chemistry Tools) according to the manufacturer's instructions, and analysed on the LSRFortessa flow cytometer using FACSDiva v.8.0 (BD Biosciences). Analysis of OP-puro incorporation was performed with FCS Express v.7.05 or FlowJo v.10.8.0.

Rex1::GFPd2 analysis

On the day of analysis, cells were trypsinized and resuspended in FACS buffer (PBS, 2% FBS and 1 mM EDTA) containing 4,6-diamidino-2-phenylindole (DAPI, 1 µg ml⁻¹). Cells were evaluated for DAPI and GFP on the LSRFortessa flow cytometer using FACSDiva v.8.0 (BD Biosciences). Viable cells were those that excluded DAPI. *Rex1::GFPd2* expression was measured by GFP mean fluorescence intensity (MFI) and quantified using FCS Express v.7.0.5 or FlowJo v.10.8.0.

Metabolic analyses

For isotope tracing experiments, ES cells were seeded in standard culture medium in six-well plates. Then, 24 h or 40 h later, cells were washed with PBS and changed into experimental medium containing a 1:1 mix of glutamine-free DMEM and glutamine-free Neurobasal medium including 10% dialysed FBS, 2-mercaptoethanol, LIF and 2 mM L-glutamine with or without 2i. The next day, cells were washed with PBS and changed into medium containing a 1:1 combination of glucose- and glutamine-free DMEM and glucose- and glutamine-free Neurobasal-A medium including 10% dialysed FBS, 2-mercaptoethanol, LIF and 2i as specified and supplemented with [¹²C]glucose (Sigma-Aldrich) and [¹²C]glutamine (Gibco) or the labelled versions of each metabolite: [¹³C]]glucose, [⁴⁻²H]glucose or [¹³C]]glutamine (Cambridge Isotope Laboratories) to a final concentration of 20 mM (glucose) and 2 mM (glutamine) for 4 h before collection. To analyse metabolites in serum/LIF+2i-cultured ES cells undergoing exit from pluripotency, ES cells were seeded in maintenance medium in six-well plates overnight. Either 24 or 40 h before collection, cells were washed with PBS and changed into medium containing a 1:1 mix of glutamine-free DMEM and Neurobasal medium including N-2 supplement, B-27 supplement, 2-mercaptoethanol and 2 mM L-glutamine. To analyse metabolites in 2i/LIF-cultured ES cells undergoing exit from pluripotency, ES cells were seeded in serum-free maintenance medium in six-well plates overnight. Either 24 or 40 h before collection, cells were washed with PBS and changed into serum-free maintenance medium without 2i or LIF. In all cases, 4 h before collecting, cells were washed with PBS and

Article

changed into medium containing a 1:1 combination of glucose- and glutamine-free DMEM and glucose- and glutamine-free Neurobasal-A medium including N-2 and B-27 supplements and 2-mercaptoethanol, and supplemented with [¹²C]glucose and [¹²C]glutamine or the labelled versions of each metabolite to a final concentration of 20 mM (glucose) and 2 mM (glutamine).

For mass spectrometry (MS) analyses of C2C12 myoblasts and NSCLC cell lines, cells were seeded in six-well plates and the medium was changed 24 h or 48 h later. The next day, the cells were washed with PBS and changed into medium containing glucose- and glutamine-free DMEM including 10% dialysed FBS and supplemented with [¹²C]glucose and [¹²C]glutamine or the labelled versions of each metabolite: [-¹³C]glucose, [^{4,2}H]glucose or [-¹³C]glutamine (Cambridge Isotope Laboratories) to a final concentration of 20 mM (glucose) and 4 mM (glutamine) for 4 h before collection. Forty-eight hours before collection, myoblasts were supplemented with 1 µg ml⁻¹ doxycycline to induce shRNA expression. For analysis of myotubes, cells seeded in six-well plates were grown to 100% confluence for 3 days, washed with PBS and changed to differentiation medium that was refreshed every day for 5 or 7 days. On the final day of differentiation, the cells were washed with PBS and changed to experimental medium described above. For analysis of C2C12 myotube genetic hairpin lines, the cells were processed as described above, but the medium was supplemented with 1 µg ml⁻¹ doxycycline for the final four days of differentiation to induce shRNA expression. Cell lines treated with inhibitors were processed as described above but medium was supplemented with DMSO, 50 µM BMS-303141, 5 mM dichloroacetate or 10 µM UK-5099 for 24 h before collection. At collection, metabolites were extracted with 1 ml ice-cold 80% methanol containing 2 µM deuterated 2-hydroxyglutarate (d-2-hydroxyglutaric-2,3,3,4,4-d₅ acid (d5-2HG)). After overnight incubation at -80 °C, lysates were collected and centrifuged at 21,000g for 20 min to remove protein. All extracts were further processed using liquid chromatography coupled with MS (LC-MS) (for analysis of the lactate/pyruvate ratio and deuterium labelling of NADH, lactate and succinate) or gas chromatography coupled with MS (GC-MS) (for all other analyses) as described below.

143B cells were plated in six-well plates; 24 h later, the medium was changed to DMEM supplemented with 10% dialysed FBS, 1 mM asparagine and DMSO or 50 µM BMS-303141. After 20 h, the medium was changed to DMEM supplemented with 10% dialysed FBS, 1 mM [-¹³C]asparagine and DMSO or 50 µM BMS-303141. The cells were extracted with 300 µl 80% methanol containing valine-D8 as an internal control. 143B extracts were further processed using LC-MS as described below.

Fatty acid analyses

To analyse fatty acids in serum/LIF+2i-cultured ES cells undergoing exit from pluripotency, ES cells were seeded in maintenance medium in six-well plates overnight. The next day, the cells were washed with PBS and changed into medium containing a 1:1 mix of glutamine-free DMEM and Neurobasal medium including N-2 supplement, B-27 supplement, 2-mercaptoethanol and 2 mM L-glutamine. Then, 24 h before collection, the cells were washed with PBS and changed into medium containing a 1:1 combination of glucose- and glutamine-free DMEM and glucose- and glutamine-free Neurobasal-A medium including N-2 supplement, B-27 supplement, 2-mercaptoethanol, 2 mM L-glutamine and 20 mM glucose supplemented with 5 mM [^{1,2}-¹³C]sodium acetate (Cambridge Isotope Laboratories). At collection, lysates were collected in PBS and centrifuged at 6,800g for 5 min to pellet the cells. To isolate fatty acids, the cell pellets were resuspended in 400 µl high-performance liquid chromatography (HPLC)-grade methanol followed by 800 µl HPLC-grade chloroform, and the samples were vortexed for 10 min at 4 °C. HPLC grade water (300 µl) was then added to induce phase separation. Next, 800 µl of the bottom chloroform layer was moved to a new tube and lyophilized. Dried samples were saponified by resuspending in 1 ml

of 80% methanol with 0.3 M KOH and heating at 80 °C for 1 h in a glass vial. HPLC grade hexanes (1 ml) were then added to the vial and briefly vortexed. Next, 800 µl of the top hexane layer was moved to a new tube and lyophilized. The extracts were then further processed by LC-MS as described below.

GC-MS analysis

The extracts were dried in an evaporator (Genevac EZ-2 Elite) and resuspended by incubating with shaking at 30 °C for 2 h in 50 µl of 40 mg ml⁻¹ methoxyamine hydrochloride in pyridine. The metabolites were further derivatized by adding 80 µl of N-methyl-N-(trimethylsilyl) trifluoroacetamide with or without 1% TCMS (Thermo Fisher Scientific) and 70 µl ethyl acetate (Sigma-Aldrich) and then incubated at 37 °C for 30 min. The samples were analysed using the Agilent 7890A gas chromatograph coupled to an Agilent 5977C mass selective detector. The gas chromatograph was operated in splitless injection mode with constant helium gas flow at 1 ml min⁻¹; 1 µl of derivatized metabolites was injected onto an HP-5ms column and the gas chromatograph oven temperature increased from 60 °C to 290 °C over 25 min. Peaks representing compounds of interest were extracted and integrated using MassHunter v.B.08 (Agilent Technologies) and then normalized to both the internal standard (d5-2HG) peak area and protein content of triplicate samples as determined using the bicinchoninic acid assay (Thermo Fisher Scientific). Steady-state metabolite pool levels were derived by quantifying the following ions: d5-2HG, 354 m/z; αKG, 304 m/z; aspartate, 334 m/z; citrate, 465 m/z; fumarate, 245 m/z; malate, 335 m/z; and succinate, 247 m/z. All of the peaks were manually inspected and verified relative to known spectra for each metabolite. Enrichment of [¹³C] or [²H] was assessed by quantifying the abundance of the following ions: aspartate, 334–346 m/z; citrate, 465–482 m/z; fumarate, 245–254 m/z; and malate, 335–347 m/z. Correction for natural isotope abundance was performed using IsoCor (v.1.0 or v.2.0)⁴². Full isotopeologue distributions generated by the isotope tracing experiments are provided in Supplementary Table 4.

LC-MS analysis

Lyophilized samples were resuspended in 80% methanol in water and transferred to LC-MS vials for measurement by LC-MS. Metabolite quantitation was performed using the Q Exactive HF-X Hybrid Quadrupole-Orbitrap Mass Spectrometer equipped with an Ion Max API source and H-ESI II probe, coupled to a Vanquish Flex Binary UHPLC system (Thermo Fisher Scientific). Mass calibrations were completed at a minimum of every 5 days in both the positive and negative polarity modes using LTQ Velos ESI Calibration Solution (Pierce).

Polar samples. Polar samples were chromatographically separated by injecting a sample volume of either 1 µl in the MS1 mode or 5 µl in the SIM mode into a SeQuant ZIC-pHILIC Polymeric column (2.1 × 150 mm, 5 mM, EMD Millipore). The flow rate was set to 150 ml min⁻¹, autosampler temperature set to 10 °C and column temperature set to 30 °C. Mobile phase A consisted of 20 mM ammonium carbonate and 0.1% (v/v) ammonium hydroxide, and mobile phase B consisted of 100% acetonitrile. The sample was gradient eluted (percentage of B) from the column as follows: 0–20 min: linear gradient from 85% to 20% B; 20–24 min: hold at 20% B; 24–24.5 min: linear gradient from 20% to 85% B; 24.5 min to the end: hold at 85% B until equilibrated with ten column volumes. Mobile phase was directed into the ion source with the following parameters: sheath gas = 45, auxiliary gas = 15, sweep gas = 2, spray voltage = 2.9 kV in the negative mode or 3.5 kV in the positive mode, capillary temperature = 300 °C, RF level = 40%, auxiliary gas heater temperature = 325 °C. Mass detection was conducted with a resolution of 240,000 in full scan mode or 120,000 in SIM mode, with an AGC target of 3,000,000 and maximum injection time of 250 ms for the full scan mode, or 100,000 ms and 100 ms for the SIM mode. Metabolites were detected over mass range of 70–1,050 m/z in full scan

positive mode, or SIM in positive mode using a quadrupole isolation window of 0.7 m/z .

Non-polar samples. Non-polar samples were chromatographically separated by injecting 2 μ l into an Accucore Vanquish C18+ column (2.1 \times 100 mm, 1.5 μ m particle size, 27101-102130, Thermo Fisher Scientific). The autosampler temperature was set at 10 °C and the flow rate was 500 μ l min $^{-1}$ with the column temperature set at 50 °C. The largely isocratic gradient consisted of a mixture of water and 5 mM ammonium acetate as A and acetonitrile as B. At 0–6.5 min, the solvent composition was held at 60% B, followed by a change to 98% B between 6.5–6.6 min. The composition was held at 98% B between 6.6–9.0 min, and then returned back to starting conditions at 60% B between 9.0–9.1 min. It was then held for an additional 4.4 min to re-equilibrate the column for the next run. Non-polar analytes were detected in the negative polarity mode at a resolution of 240,000 in the full scan setting, using a mass range of 240–650 m/z . The AGC target value was 3,000,000 with a maximum injection time of 200 ms. The chromatography peak width setting was 10 s (FWHM), and data were collected in profile mode. The parameters for the H-ESI source were as follows: sheath gas flow rate of 53 units, aux gas flow rate of 14 units, sweep gas flow rate of 3 units, with the spray voltage set at 3.00 kV. The funnel RF level was set at 40%, and the capillary and auxiliary gas heater temperatures were held at 300 °C and 400 °C, respectively. Quantification of all metabolites was performed using Tracefinder v.4.1 (Thermo Fisher Scientific) referencing an in-house metabolite standards library using \leq 5 ppm mass error. Data from stable isotope labelling experiments include correction for natural isotope abundance using IsoCor v.2.2. Isotopologue distributions are provided in Supplementary Table 4.

Oxygen consumption

The oxygen consumption rate (OCR) was measured using a Seahorse XFe96 Extracellular Flux Analyzer (Agilent Technologies). ES cells were plated on gelatin-coated tissue-culture-treated XF96 96-well plates (Agilent Technologies) at 2 \times 10 4 cells per well in standard maintenance medium. The next day, the cells were washed twice with assay medium (Seahorse XF DMEM medium supplemented with 10 mM glucose) and changed to assay medium containing 2 mM L-glutamine for 2 h before the assay. Baseline measurements of OCR were obtained three times. After the assay, the protein content was determined and averaged for each condition and the OCR measurements were normalized to these values. The third baseline OCR reading was averaged across all 12 replicates; averaged values from three independent experiments are shown.

Western blotting

Protein lysates were extracted in 1× RIPA buffer (Cell Signaling Technology), separated by SDS–polyacrylamide gel electrophoresis and transferred to nitrocellulose membranes (Bio-Rad). For histone blots, cell pellets were flash-frozen in ethanol and resuspended in Laemmli buffer for sonication. The samples were mixed with 5% BME and 0.01% bromophenol blue before identical separation was performed as described for protein lysates. The membranes were blocked in 3% milk in Tris-buffered saline with 0.1% Tween-20 (TBST) or 5% BSA in TBST and incubated at 4 °C with primary antibodies overnight. After TBST washes the next day, the membranes were incubated with horseradish-peroxidase-conjugated secondary antibodies (mouse, NA931; rabbit, NA934; Cytiva) for at least 2 h, incubated with enhanced chemiluminescence (Thermo Fisher Scientific) and imaged using the SRX-101A X-ray Film Processor (Konica Minolta). The antibodies used (at 1:1,000 unless otherwise indicated) were: anti-ACL (4332; Cell Signaling Technologies), anti-ACO2 (MA1-029; Thermo Fisher Scientific), anti-SLC25A1 (15235-1-AP; ProteinTech), anti-MDH1 (sc-166879; Santa Cruz Biotechnology), anti-AceCS1/ACSS2 (3658; Cell Signaling Technologies), anti-TCF7L1 (sc-166411; Santa Cruz Biotechnology), anti-myogenin/MYOG (14-5643-82; Thermo Fisher Scientific), anti-MYH3 (22287-1-AP; ProteinTech), anti-vinculin (1:10,000;

V9131; Sigma), anti-tubulin (T9026; Sigma-Aldrich), anti-H3K9ac (9469; Cell Signaling Technology), anti-H3K14ac (07-353; Millipore Sigma), anti-H3K27ac (39133; Active Motif), anti-H4K16ac, (1:500; 39167; Active Motif), anti-H3 (Ab1791; Abcam) and anti-H4 (1:500; 07-108; Millipore Sigma). C2C12 myoblast genetic hairpin lines were maintained in medium supplemented with 1 μ g ml $^{-1}$ doxycycline for 48 h before protein lysate extraction to induce shRNA expression.

Colony-formation assay

ES cells adapted to 2i/LIF or serum/LIF+2i were subjected to exit from pluripotency in triplicate for 12, 24 or 40 h. On the day of collection, the cells were counted and reseeded at a density of 2,000 cells per well in technical triplicate in maintenance medium containing 2i and LIF. The medium was refreshed every 3 days. Then, 6 days after initial seeding, the cells were fixed with citrate/acetone/3% formaldehyde for 30 s and stained with the Leukocyte Alkaline Phosphatase Kit (Sigma-Aldrich) according to the manufacturer's instructions. The colonies were quantified using ImageJ's particle analysis function and technical triplicates were averaged for each condition.

Quantification of gene expression

RNA was isolated from six- or twelve-well plates using TRIzol (Invitrogen) according to the manufacturer's instructions and 200 ng RNA was used for complementary DNA (cDNA) synthesis using the iScript cDNA Synthesis Kit (Bio-Rad). Quantitative PCR with reverse transcription (RT-qPCR) analysis was performed in technical triplicate using QuantStudio 5 or 6 Flex (Applied Biosystems) with the Power SYBR Green Master Mix (Thermo Fisher Scientific). All data were generated using cDNA from three independent wells for each condition. Actin was used as an endogenous control for all of the experiments. A list of the RT-qPCR primer sequences is provided in Supplementary Table 2.

RNA-seq analysis of myoblasts and myotubes

RNA was isolated as described above and quantified using a Qubit 3.0 fluorometer. RNA-seq libraries were generated using the TruSeq Stranded mRNA Library Prep Kit (20020594, Illumina) according to the manufacturer's instructions. The samples were pooled and sequenced at the Memorial Sloan Kettering Cancer Center Integrated Genomics Operation. RNA-seq libraries were filtered and trimmed using fastp⁴³ and mapped with STAR aligner⁴⁴ against the mm10 mouse genome assembly using default parameters. featureCounts⁴⁵ was used to calculate gene counts for input into DESeq2 (ref. ⁴⁶) for quality control analysis, size normalization and variance dispersion corrections.

Statistics and reproducibility

Prism 9 (GraphPad) software was used for statistical analyses, except for DepMap data. Error bars, P values and statistical tests are reported in the figures and figure legends. Statistical analyses on DepMap data were performed using Python v3.8. No statistical methods were used to predetermine sample sizes. All data were collected and analyzed objectively using instruments without bias. Therefore, blinding is not relevant to this study. Experimental samples were randomly distributed into groups. Experiments were performed in biological triplicate or as indicated in the figure legends and were repeated at least two (often many more) times.

Reporting summary

Further information on research design is available in the Nature Research Reporting Summary linked to this paper.

Data availability

RNA-seq data supporting the findings of this study have been deposited in the Gene Expression Omnibus under the accession code GSE183434. Alignment was performed against the mouse mm10 genome assembly.

Article

Gene essentiality data and NSCLC gene expression data are available from the DepMap Portal (<https://depmap.org/portal/>). Isotopologue distributions from all MS isotope tracing experiments are provided in Supplementary Table 4. Source data are provided with this paper.

Code availability

The code used to perform gene essentiality correlation and network modelling is provided at GitHub (<https://github.com/finley-lab/coessentiality-network>).

29. Dempster, J. M. et al. Extracting biological insights from the project achilles genome-scale CRISPR screens in cancer cell lines. Preprint at <https://doi.org/10.1101/720243> (2019).
30. Meyers, R. M. et al. Computational correction of copy number effect improves specificity of CRISPR-Cas9 essentiality screens in cancer cells. *Nat. Genet.* **49**, 1779–1784 (2017).
31. Ashburner, M. et al. Gene ontology: tool for the unification of biology. The Gene Ontology Consortium. *Nat. Genet.* **25**, 25–29 (2000).
32. The Gene Ontology Consortium. The Gene Ontology Resource: 20 years and still GOing strong. *Nucleic Acids Res.* **47**, D330–D338 (2019).
33. Virtanen, P. et al. SciPy 1.0: fundamental algorithms for scientific computing in Python. *Nat. Methods* **17**, 261–272 (2020).
34. Ghandi, M. et al. Next-generation characterization of the Cancer Cell Line Encyclopedia. *Nature* **569**, 503–508 (2019).
35. Subramanian, A. et al. Gene set enrichment analysis: a knowledge-based approach for interpreting genome-wide expression profiles. *Proc. Natl Acad. Sci. USA* **102**, 15545–15550 (2005).
36. Carey, B. W., Finley, L. W., Cross, J. R., Allis, C. D. & Thompson, C. B. Intracellular α-ketoglutarate maintains the pluripotency of embryonic stem cells. *Nature* **518**, 413–416 (2015).
37. Dow, L. E. et al. Inducible *in vivo* genome editing with CRISPR-Cas9. *Nat. Biotechnol.* **33**, 390–394 (2015).
38. Ran, F. A. et al. Genome engineering using the CRISPR-Cas9 system. *Nat. Protoc.* **8**, 2281–2308 (2013).
39. MacDougall, M. S., Clarke, R. & Merrill, B. J. Intracellular Ca²⁺ homeostasis and nuclear export mediate exit from naive pluripotency. *Cell Stem Cell* **25**, 210–224 (2019).
40. Morris, J. P. T. et al. α-Ketoglutarate links p53 to cell fate during tumour suppression. *Nature* **573**, 595–599 (2019).
41. Fellmann, C. et al. An optimized microRNA backbone for effective single-copy RNAi. *Cell Rep.* **5**, 1704–1713 (2013).

42. Millard, P. et al. IsoCor: isotope correction for high-resolution MS labeling experiments. *Bioinformatics* **35**, 4484–4487 (2019).
43. Chen, S., Zhou, Y., Chen, Y. & Gu, J. fastp: an ultra-fast all-in-one FASTQ preprocessor. *Bioinformatics* **34**, i884–i890 (2018).
44. Dobin, A. et al. STAR: ultrafast universal RNA-seq aligner. *Bioinformatics* **29**, 15–21 (2013).
45. Liao, Y., Smyth, G. K. & Shi, W. featureCounts: an efficient general purpose program for assigning sequence reads to genomic features. *Bioinformatics* **30**, 923–930 (2014).
46. Love, M. I., Huber, W. & Anders, S. Moderated estimation of fold change and dispersion for RNA-seq data with DESeq2. *Genome Biol.* **15**, 550 (2014).

Acknowledgements We thank the members of the Finley laboratory for discussion, and A. Boire, A. Intlekofer, S. Vardhana, E. Reznik and K. S. Tan for feedback. *Rex1::GFPd2* cells were a gift from A. Smith. P.K.A. is an NICHD Ruth L. Kirschstein Predoctoral fellow (F31HD098824). B.T.J. is a Gerstner Sloan Kettering Grayer Fellow and is supported by a Medical Scientist Training Program grant from the NIGMS of the National Institutes of Health under award number T32GM007739 to the Weill Cornell/Rockefeller/Sloan Kettering Tri-Institutional MD-PhD Program. K.I.P. is supported by a Bruce Charles Forbes Pre-Doctoral Fellowship (MSKCC). J.S.B. is supported by a Human Frontier Science Program Fellowship (LT000200/2021-L). L.B.S. is supported by R00CA218679 and P30CA015704. L.W.S.F. is a Searle Scholar. This research was also supported by grants to L.W.S.F. from the Pershing Square Sohn Prize for Cancer Research, the Starr Foundation (I2-0051), the NIH/NCI (R37 CA252305) and the Anna Fuller Fund as well as the Memorial Sloan Kettering Cancer Center Support Grant P30CA008748.

Author contributions P.K.A. and L.W.S.F. conceived the study. P.K.A. and B.T.J. performed all of the experiments with assistance from K.I.P., J.S.B. and J.E.; M.L.H., O.J.N. and S.P.A. performed LC-MS experiments under the guidance of L.B.S.; B.T.J. performed genetic co-essentiality mapping and network modelling with guidance from E.D. K.I.P. performed RNA-seq. L.B.S. provided additional study guidance. L.W.S.F. supervised the project. P.K.A. and L.W.S.F. wrote the manuscript with input from all of the authors.

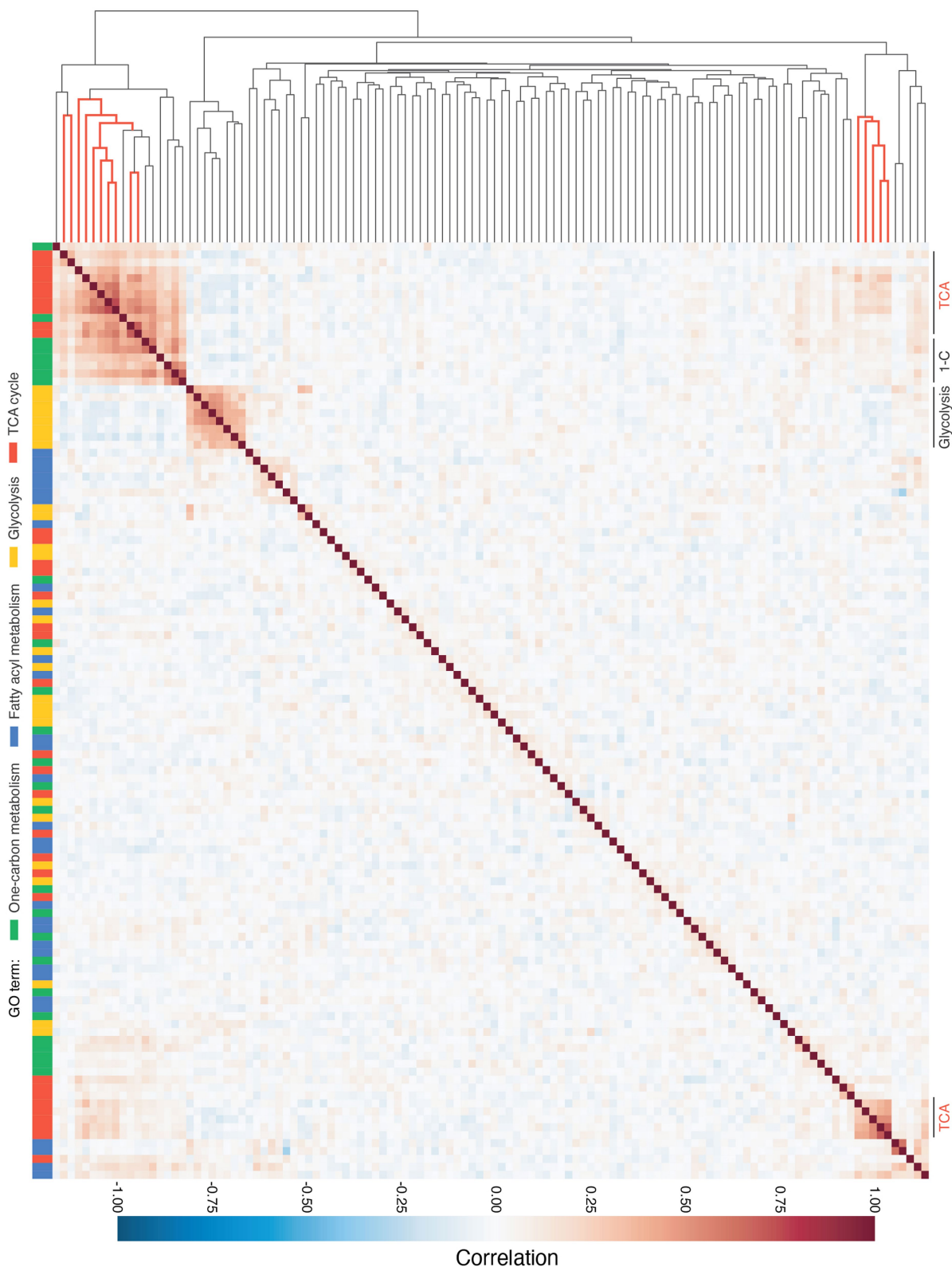
Competing interests P.K.A., B.T.J. and L.W.S.F. are listed as inventors on a provisional patent application (US provisional application no. 63/272,940) filed by the Memorial Sloan Kettering Cancer Center. The patent application covers the use of ACL inhibitors to modify the self-renewal potential of ES cells. The other authors declare no competing interests.

Additional information

Supplementary information The online version contains supplementary material available at <https://doi.org/10.1038/s41586-022-04475-w>.

Correspondence and requests for materials should be addressed to Lydia W. S. Finley. **Peer review information** *Nature* thanks the anonymous reviewers for their contribution to the peer review of this work. Peer reviewer reports are available.

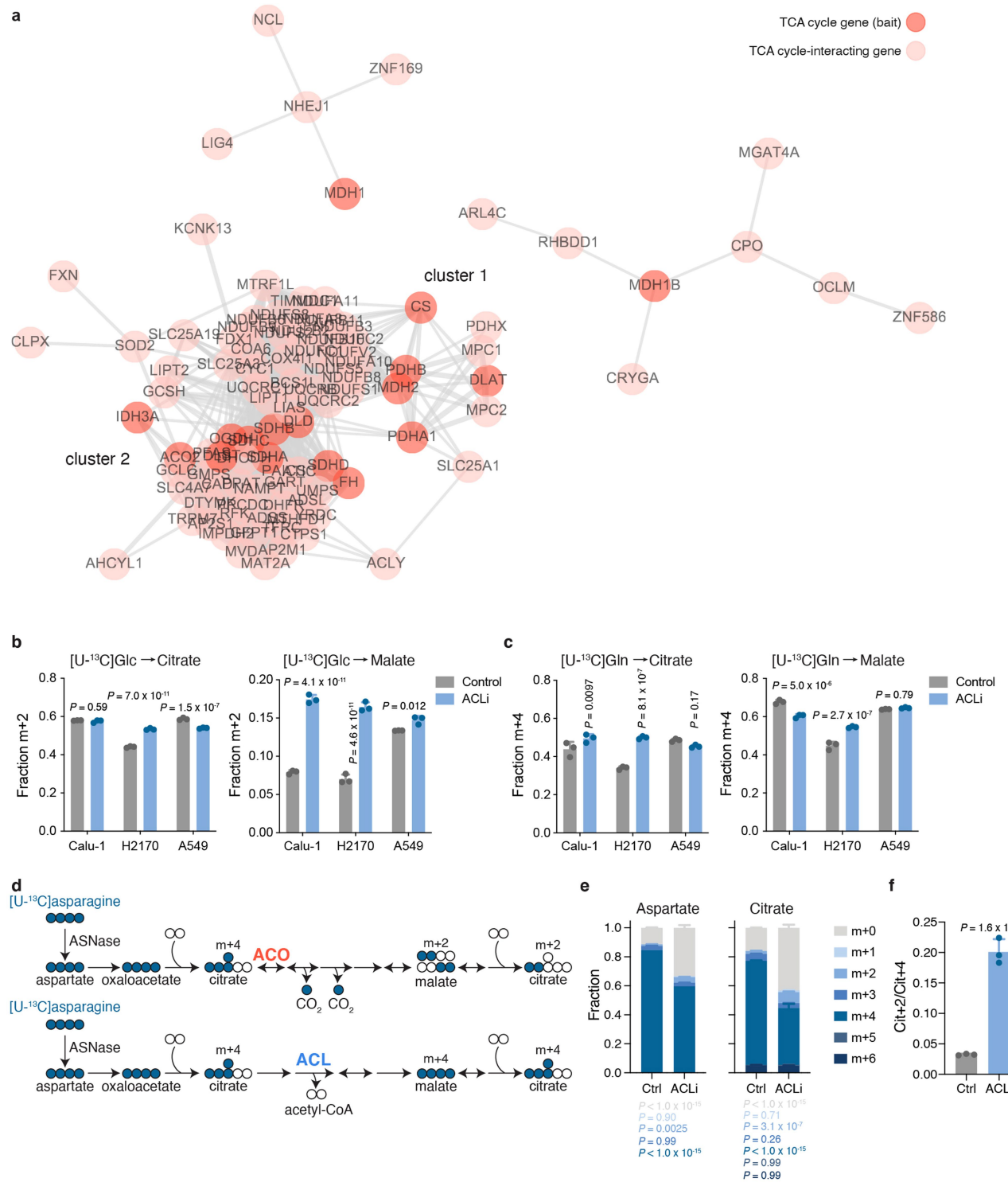
Reprints and permissions information is available at <http://www.nature.com/reprints>.



Extended Data Fig. 1 | Metabolic gene essentiality correlations across cancer cell lines. Heatmap depicting hierarchical clustering of pairwise gene essentiality score correlations of core metabolic pathway genes derived from four GO terms: tricarboxylic acid (TCA) cycle, canonical glycolysis, one-carbon

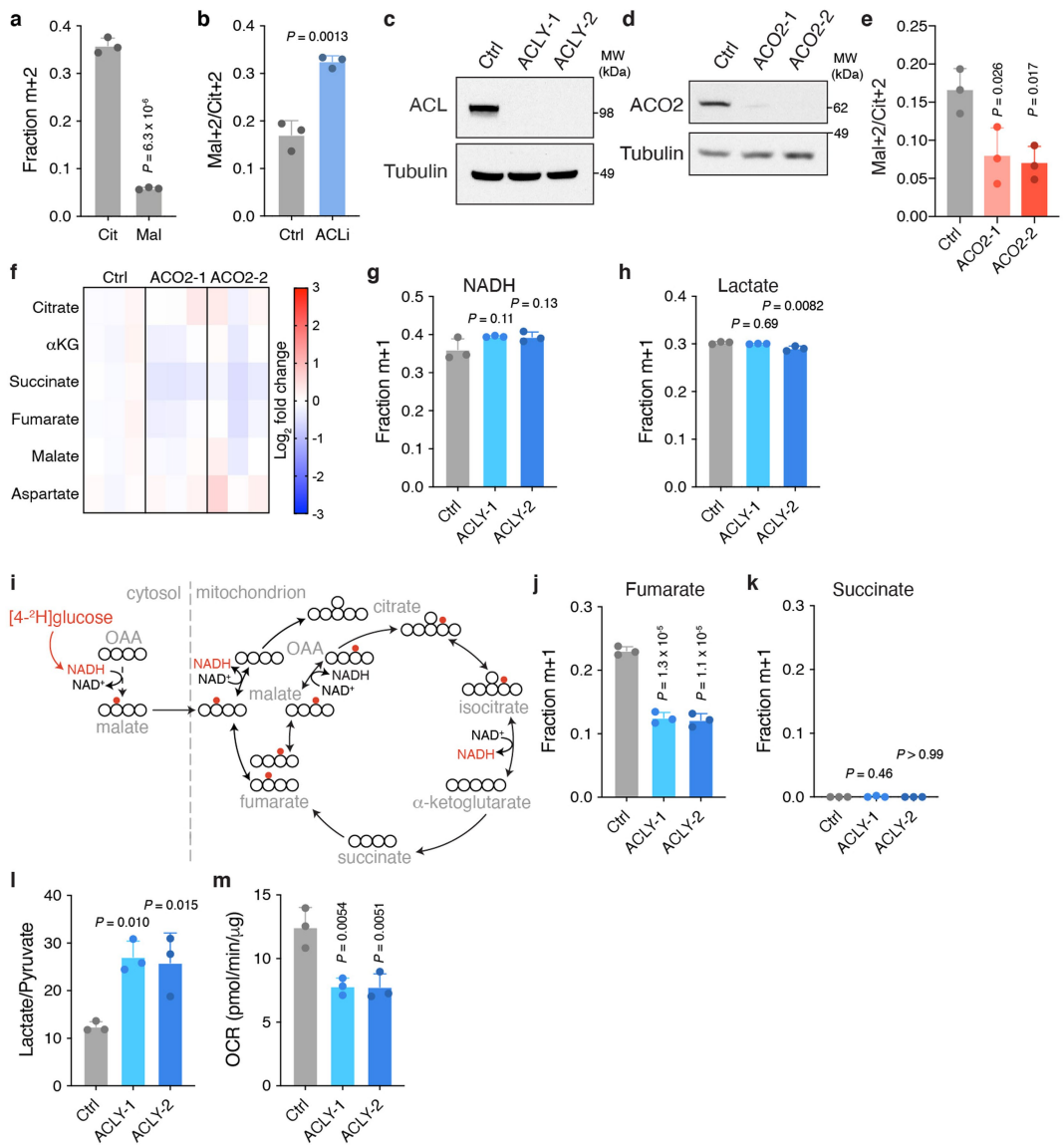
metabolic process and fatty-acyl-CoA metabolic process. Genes are colour coded to the left of the heatmap according to the GO term. TCA cycle genes are highlighted (red) in the dendrogram. Gene names and correlation scores can be found in Supplementary Table 1.

Article



Extended Data Fig. 2 | Effect of ACL inhibition on ¹³C labelling of TCA cycle metabolites. **a**, Two-dimensional network diagram representing gene essentiality score correlations between TCA cycle genes and their top co-dependencies. The strength of the correlation between genes is represented by both the length and thickness of the connecting edge. Correlation scores are shown in Supplementary Table 1. **b, c**, Fractional enrichment of citrate (left) and malate (right) in three NSCLC cell lines cultured in medium containing [¹³C]glucose (**b**) or [¹³C]glutamine (**c**) and treated with vehicle or 50 μM BMS-303141 (ACLi) for 24 h. **d**, Schematic depicting [¹³C]asparagine labelling of aspartate and citrate in cells expressing guinea pig asparaginase (ASNase). Asparagine-derived aspartate will generate

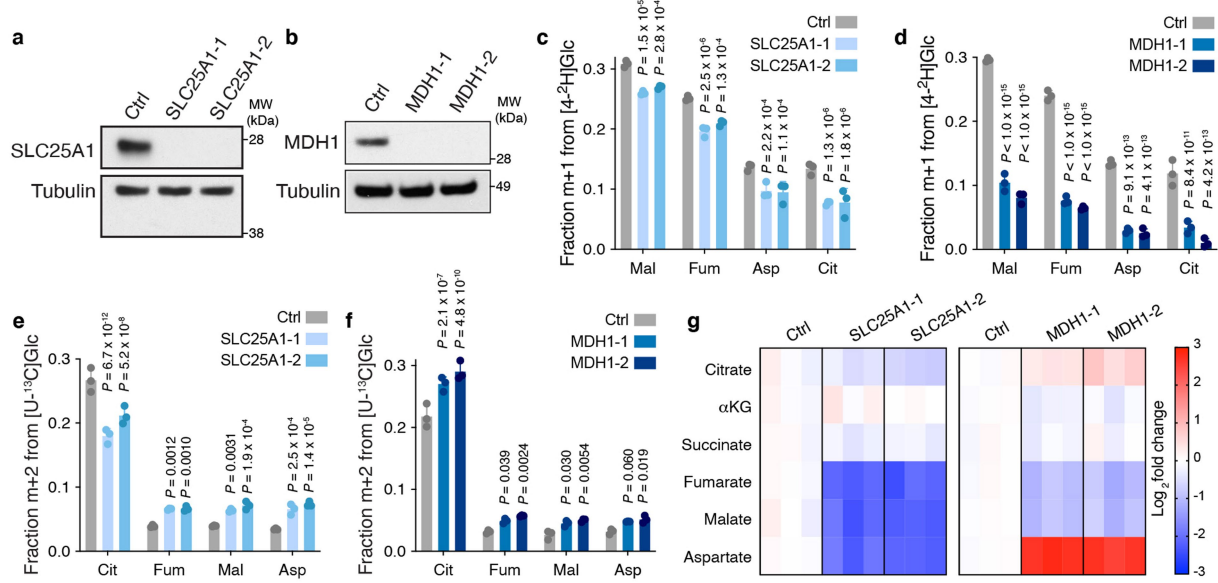
M+4-labelled citrate. Top, M+4-labelled citrate metabolized via the canonical TCA cycle will lose two labelled carbons as CO₂, ultimately regenerating citrate that retains two labelled carbons (M+2). Bottom, M+4-labelled citrate metabolized by ACL will yield M+4 labelled oxaloacetate that will ultimately regenerate M+4-labelled citrate. **e, f**, Fractional labelling of aspartate (left) and citrate (right) (**e**) or citrate M+2 relative to citrate M+4 (cit+2/cit+4) (**f**) in ASNase-expressing 143B human osteosarcoma cells cultured in medium containing [¹³C]asparagine and treated with vehicle or 50 μM ACLi for 24 h. Data are mean ± SD, n = 3 independent replicates. Significance was assessed in comparison to vehicle treatment by two-way ANOVA with Sidak's multiple comparisons post-test (**b–c, e**) or using unpaired two-tailed Student's t-test (**f**).



Extended Data Fig. 3 | ACO2 and ACL disruption in embryonic stem cells.

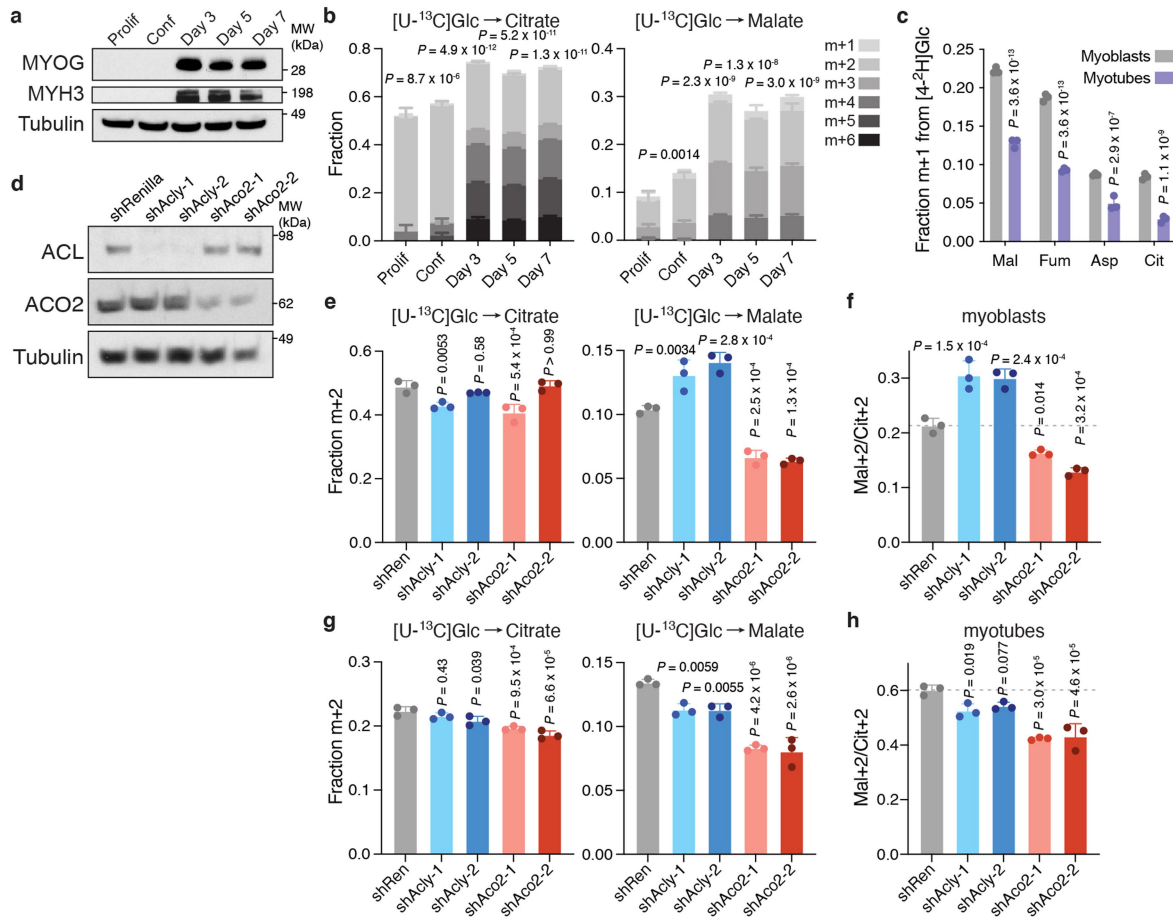
a, Fractional M+2 enrichment of citrate and malate in mouse ES cells cultured in medium containing [^{13}C]glucose. **b**, Fractional enrichment of malate M+2 relative to citrate M+2 (mal+2/cit+2) derived from [^{13}C]glucose in ES cells following treatment with vehicle or 50 μM BMS-303141 (ACLi) for 24 h. **c**, Immunoblot of clonal mouse ES cells in which CRISPR/Cas9-mediated editing was used to target either a non-genic region of chromosome 8 (Ctrl) and *Acy* (ACLY-1 and ACLY-2) (**c**) or *Aco2* (ACO2-1 and ACO2-2) (**d**). **e, f**, Assessment of the [^{13}C]glucose-derived mal+2/cit+2 ratio (**e**) or steady-state levels of TCA cycle metabolites represented as the fold change (expressed in \log_2) relative to Ctrl (**f**) in control and *Aco2*-edited ES cells. **g, h, j, k**, Fractional M+1 enrichment of

NADH (**g**), lactate (**h**), fumarate (**j**) and succinate (**k**) in control and *Acy*-edited ES cells cultured in medium containing [$4\text{-}^{2}\text{H}$]glucose. **i**, Schematic depicting deuterium transfer from [$4\text{-}^{2}\text{H}$]glucose first onto malate in the cytoplasm then onto TCA cycle metabolites in the mitochondria. **l**, Quantification of the lactate over pyruvate ratio in control and *Acy*-edited ES cells. **m**, The baseline oxygen consumption rate (OCR) in control and *Acy*-edited ES cells normalized to protein content. Twelve technical replicates were averaged for each of three independent experiments. Data are mean \pm SD, $n = 3$ independent replicates unless otherwise noted. Significance was assessed using unpaired two-tailed Student's *t*-test (**a, b**) or comparison to control cells by one-way ANOVA with Sidak's multiple comparisons post-test for all other panels.



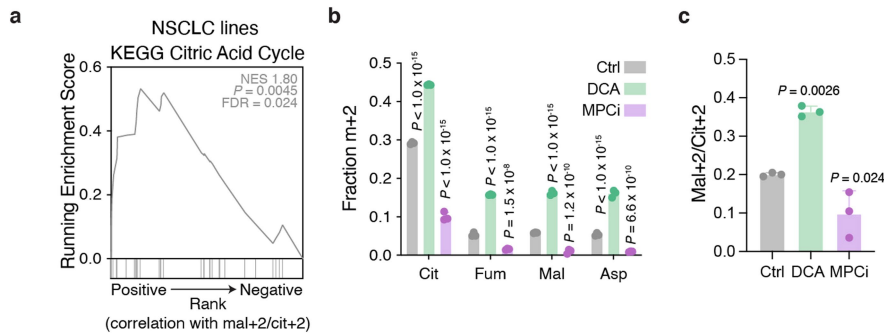
Extended Data Fig. 4 | SLC25A1 and MDH1 contribute to TCA cycle metabolism in embryonic stem cells. **a, b**, Immunoblot of clonal mouse ES cells in which CRISPR/Cas9-mediated editing was used to target either a non-genic region of chromosome 8 (Ctrl) and *Slc25a1* (SLC25A1-1 and SLC25A1-2) (**a**) or *Mdh1* (MDH1-1 and MDH1-2) (**b**). **c, d**, Fractional M+1 enrichment of malate (Mal), fumarate (Fum), aspartate (Asp) and citrate (Cit) in control (Ctrl) and *Slc25a1*-edited ES cells (**c**) or *Mdh1*-edited ES cells (**d**) cultured in medium containing [4^2H]glucose. **e, f**, Fractional M+2 enrichment of citrate,

fumarate, malate and aspartate derived from [U^{13}C]glucose in control and *Slc25a1*-edited (**e**) or *Mdh1*-edited (**f**) ES cells. **g**, Steady-state levels of TCA cycle metabolites in *Slc25a1*-edited or *Mdh1*-edited ES cells. Levels are represented as the fold change (expressed in \log_2) relative to chromosome 8-targeted control cells. Data are mean \pm SD, $n = 3$ independent replicates. Significance was assessed in comparison to control cells by two-way ANOVA (**c-f**) with Sidak's multiple comparisons post-test.



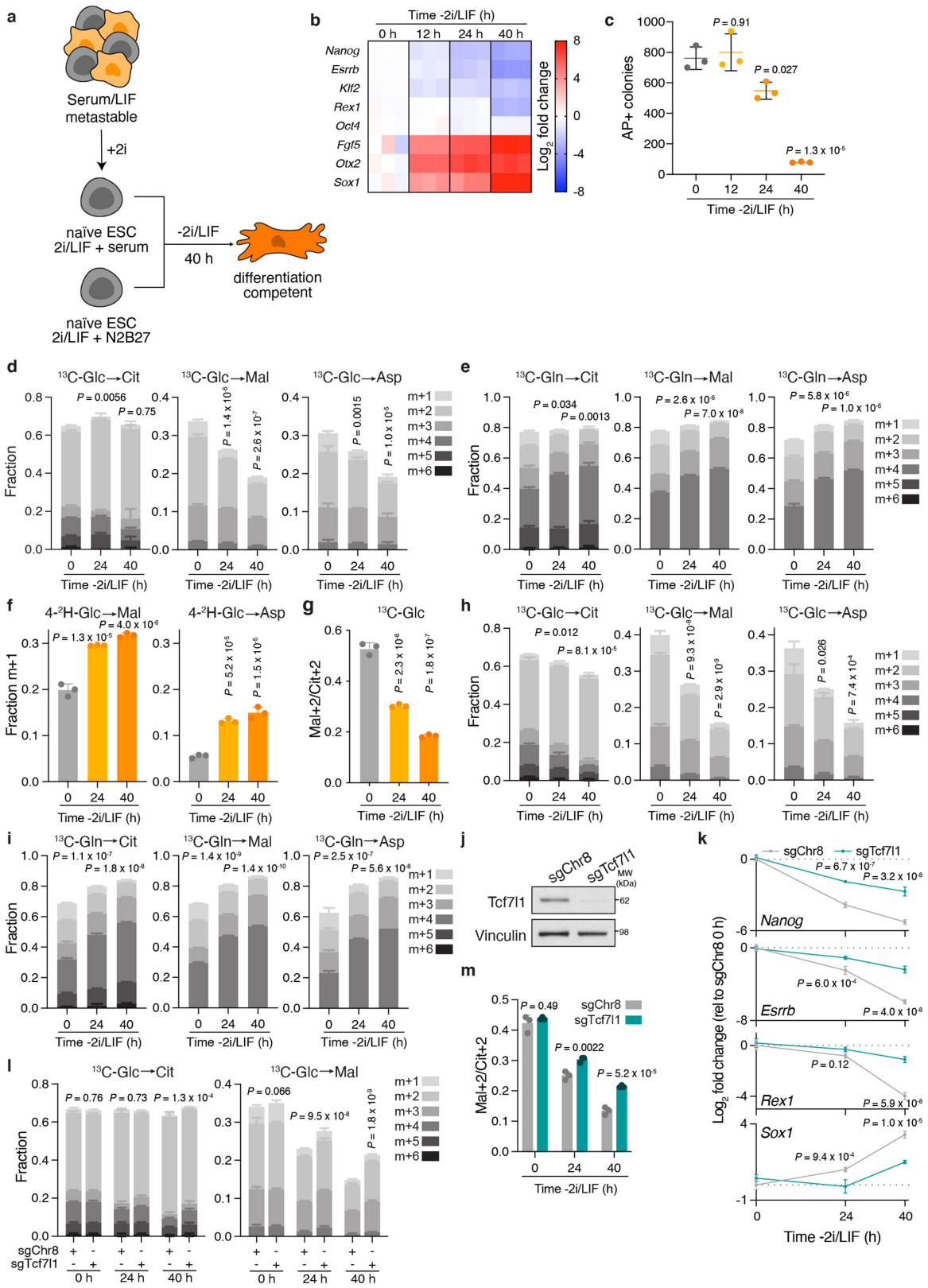
Extended Data Fig. 5 | Effect of myogenic differentiation on ¹³C-glucose labelling of TCA cycle intermediates. **a**, Immunoblot comparing expression of myogenesis markers MYOG and MYH3 between proliferating (Prolif) and 100% confluent (Conf) myoblasts and myotubes differentiated for 3, 5 or 7 days. **b**, Fractional labelling of citrate (left) and malate (right) in proliferating and confluent myoblasts and myotubes differentiated for 3, 5 or 7 days cultured in medium containing [$U-^{13}\text{C}$]glucose. **c**, Fractional M+1 enrichment from [4-²H]glucose of malate (Mal), fumarate (Fum), aspartate (Asp) and citrate (Cit) in myoblasts and myotubes differentiated for 5 days. **d**, Immunoblot comparing expression of ACL and ACO2 in C2C12 cells expressing doxycycline-inducible shRNAs targeting *Acly* (shAcly-1 and shAcly-2), *Aco2* (shAco2-1 and shAco2-2) or Renilla luciferase (shRen, used as a control). Cells were cultured on doxycycline

for two days to induce shRNA expression. **e-h**, Fractional M+2 enrichment of citrate (left) and malate (right) or malate M+2 relative to citrate M+2 (mal+2/cit+2) in myoblasts (**e,f**) or myotubes (**g,h**) expressing doxycycline-inducible shRNAs targeting *Acly*, *Aco2* or Renilla luciferase cultured in medium containing [$U-^{13}\text{C}$]glucose. Myoblasts and myotubes were cultured on doxycycline for 2 or 4 days, respectively, to induce shRNA expression. Data are mean \pm SD, $n = 3$ independent replicates. In **b**, significance was assessed using one-way ANOVA with Sidak's multiple comparisons post-test to compare total metabolite fraction labelled relative to proliferating myoblasts. In remaining panels, significance was assessed by two-way ANOVA in comparison to myoblasts (**c**) or by one-way ANOVA in comparison to shRen-expressing myoblasts (**e-f**) or myotubes (**g-h**) with Sidak's multiple comparisons post-test.



Extended Data Fig. 6 | Transcriptional profiles associated with TCA cycle choice. **a**, Gene set enrichment analysis showing that genes positively correlated with fractional enrichment of malate M+2 relative to citrate M+2 (mal+2/cit+2) derived from [$U-^{13}C$]glucose in 68 NSCLC cell lines are enriched for KEGG citric acid (TCA) cycle-associated genes. **b, c**, Fractional M+2 enrichment of citrate (Cit), fumarate (Fum), malate (Mal) and aspartate (Asp)

(**b**) or mal+2/cit+2 (**c**) derived from [$U-^{13}C$]glucose in mouse ES cells following treatment with vehicle, 5 mM DCA or 10 μ M MPCi for 24 h. Data are mean \pm SD, $n = 3$ independent samples. In **b-c**, significance was assessed in comparison to vehicle treatment by two-way ANOVA (**b**) or one-way ANOVA (**c**) with Sidak's multiple comparisons post-test.



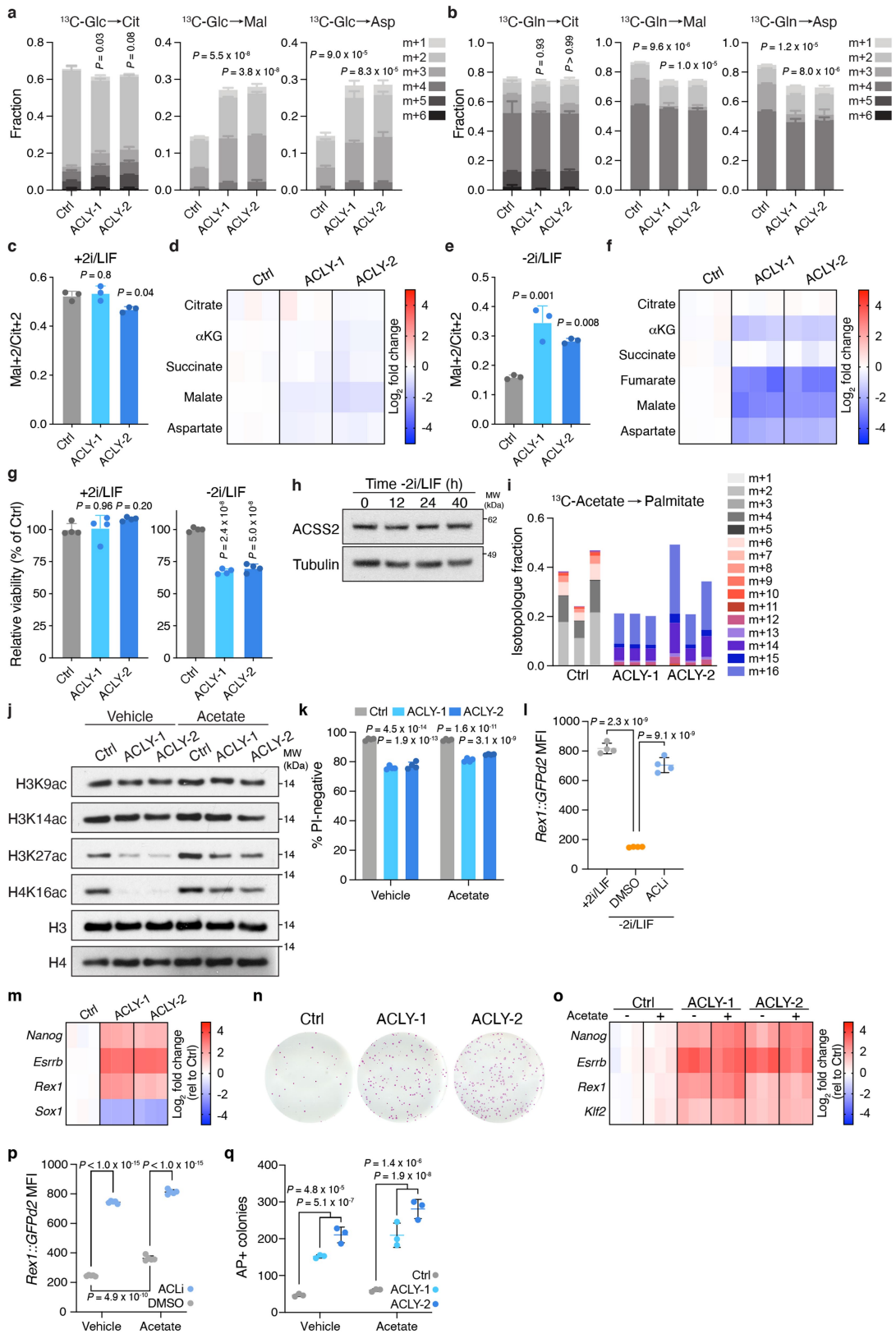
Extended Data Fig. 7 | See next page for caption.

Article

Extended Data Fig. 7 | ACL loss blunts exit from naive pluripotency.

a, Experimental setup for cell fate transitions. Mouse ES cells cultured in serum and leukemia inhibitory factor (LIF) are a heterogenous population that can be converted to the naive, ground state of pluripotency by addition of MEK and GSK3 β inhibitors (2i) in either serum replete (serum/LIF+2i, **d-f**) or serum-free (2i/LIF, **g-i**) media formulations. Transition to serum-free medium lacking 2i/LIF (-2i/LIF) induces exit from the naive pluripotent state, enabling ES cells to gain differentiation competence. **b**, RT-qPCR of pluripotency-associated (*Nanog*, *Esr1*, *Klf2*, *Rex1* and *Oct4*) and early differentiation-associated (*Fgf5*, *Otx2* and *Sox1*) genes in 2i/LIF-cultured ES cells subjected to 2i/LIF withdrawal for 12, 24 or 40 h. Levels are represented as the fold change (expressed in log₂) relative to naive, 2i/LIF-cultured ES cells (0 h). **c**, Quantification of alkaline phosphatase (AP)-positive colonies representing ES cells that failed to exit from the pluripotent state. 2i/LIF-cultured ES cells were subjected to 2i/LIF withdrawal for 0, 12, 24 or 40 h and then reseeded at clonal density into medium containing 2i and LIF. **d-f**, Fractional labelling of citrate (Cit), malate (Mal) and aspartate (Asp) in serum/LIF+2i-cultured ES cells incubated with [¹³C]glucose (**d**), [¹³C]glutamine (**e**) or [⁴H]glucose (**f**) subjected to exit from pluripotency for the indicated times. **g**, Fractional enrichment of glucose-derived malate M+2 relative to citrate M+2 (mal+2/cit+2) in 2i/LIF-cultured ES cells subjected to 2i/LIF withdrawal for the indicated times. **h-i**, Fractional

labelling of citrate, malate and aspartate in 2i/LIF-cultured ES cells cultured in medium containing [¹³C]glucose (**h**) or [¹³C]glutamine (**i**) subjected to 2i/LIF withdrawal for the indicated times. **j**, Immunoblot of polyclonal ES cells in which CRISPR/Cas9-mediated editing was used to target either a non-genic region of chromosome 8 (sgChr8) or *Tcf7l1* (sgTcf7l1). **k**, RT-qPCR of pluripotency-associated (*Nanog*, *Esr1*, and *Rex1*) and early differentiation-associated (*Sox1*) genes in control and *Tcf7l1*-edited ES cells adapted to the naive, ground state and subjected to 2i/LIF withdrawal for the indicated times. Levels are represented as the fold change (expressed in log₂) relative to chromosome 8-targeted control cells in the naive, ground state (0 h). **l-m**, Fractional labelling of citrate (left) and malate (right) (**l**) and glucose-derived mal+2/cit+2 ratio (**m**) in chromosome 8-targeted control or *Tcf7l1*-edited ES cells cultured in medium containing [¹³C]glucose subjected to 2i/LIF withdrawal for the indicated times. Data are mean \pm SD, $n = 3$ independent replicates. In **d-e**, **h-i**, and **l**, significance was assessed using one-way ANOVA (**d-e**, **h-i**) or two-way ANOVA (**l**) with Sidak's multiple comparisons post-test to compare total metabolite fraction labelled relative to the 0 h timepoint (**d-e**, **h-i**) or control cells (**l**). In remaining panels, significance was assessed relative to the 0 h timepoint using one-way ANOVA (**c**, **f-g**) or chromosome 8-targeted control cells at each time point using two-way ANOVA (**k**, **m**) with Sidak's multiple comparisons post-test.

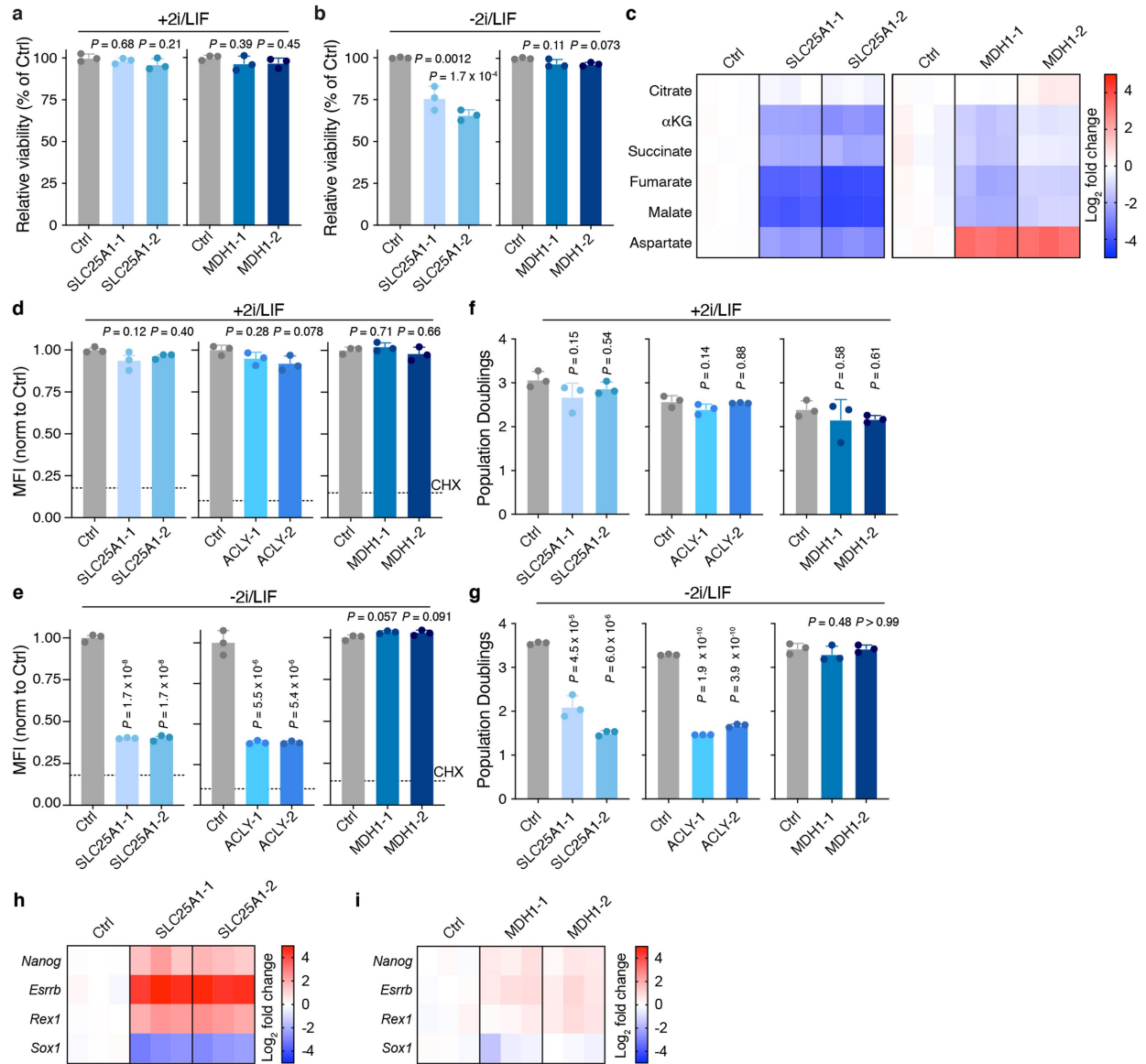


Extended Data Fig. 8 | See next page for caption.

Article

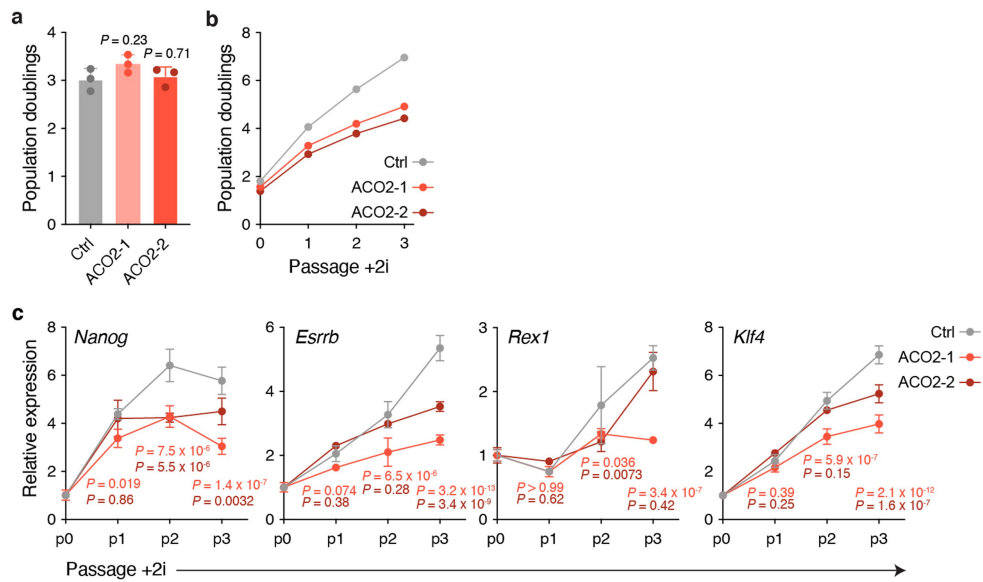
Extended Data Fig. 8 | Acetate does not reverse the effects of ACL loss on exit from pluripotency. **a, b**, Fractional labelling of citrate (Cit), malate (Mal) and aspartate (Asp) in control and *Acly*-edited ES cells cultured in medium containing [$U\text{-}^{13}\text{C}$]glucose (**a**) or [$U\text{-}^{13}\text{C}$]glutamine (**b**) following 40 h of 2i/LIF withdrawal. **c, d**, Fractional enrichment of malate M+2 relative to citrate M+2 (mal+2/cit+2) derived from [$U\text{-}^{13}\text{C}$]glucose (**c**) or steady-state levels of TCA cycle metabolites (**d**) in naive, 2i-adapted control (Ctrl) and *Acly*-edited (ACLY-1 and ACLY-2) ES cells. Steady-state levels are represented as the fold change (expressed in log₂) relative to control cells. **e, f**, Assessment of the [$U\text{-}^{13}\text{C}$]glucose-derived mal+2/cit+2 ratio (**e**) and steady-state levels of TCA cycle metabolites (**f**) in control and *Acly*-edited ES cells subjected to 2i/LIF withdrawal for 40 h. **g**, Relative viability (measured by PI exclusion) of control and *Acly*-edited ES cells maintained in the naive pluripotent state (+2i/LIF, left) or subjected to 2i/LIF withdrawal for 40 h (-2i/LIF, right). **h**, Immunoblot showing expression of ACSS2, the enzyme that converts acetate to acetyl-CoA in the cytosol, in naive, ground state ES cells subjected to 2i/LIF withdrawal for the indicated times. **i**, Fractional labelling of palmitate in control and *Acly*-edited ES cells cultured in medium containing [$U\text{-}^{13}\text{C}$]acetate following 40 h of 2i/LIF withdrawal. Each bar represents one independent sample. **j**, Immunoblot comparing levels of acetylation (ac) at indicated histone lysine residues in control and *Acly*-edited ES cells subjected to 2i/LIF withdrawal for 40 h in the presence of vehicle or 5 mM sodium acetate. **k**, Relative viability of control and *Acly*-edited ES cells subjected to 2i/LIF withdrawal for 40 h in the presence of vehicle or 5 mM sodium acetate. **l**, Quantification of GFP mean fluorescence intensity (MFI) encoded by the *Rex1::GFPd2* reporter in ES cells subjected to 2i/LIF withdrawal for 40 h in the presence of vehicle or 50 μM BMS-303141 (ACLi). Naïve ES cells (+2i/LIF) are included as a control. Representative histograms are

shown in Fig. 4d. **m**, RT-qPCR of pluripotency-associated (*Nanog*, *Esrrb* and *Rex1*) and early differentiation-associated (*Sox1*) genes in control and *Acly*-edited ES cells subjected to 2i/LIF withdrawal for 40 h. Levels are represented as the fold change (expressed in log₂) relative to chromosome 8-targeted control cells. **n**, Alkaline phosphatase (AP) staining of colony formation assay representing control and *Acly*-edited ES cells that failed to exit the naive pluripotent state. 2i-adapted ES cells were subjected to 2i/LIF withdrawal for 40 h and then reseeded at clonal density into medium containing 2i/LIF. Quantification is shown in Fig. 4e. **o**, RT-qPCR of pluripotency-associated genes in control and *Acly*-edited ES cells subjected to 2i/LIF withdrawal for 40 h in the presence of vehicle or 5 mM sodium acetate. **p**, Quantification of GFP MFI encoded by the *Rex1::GFPd2* reporter in ES cells subjected to 2i/LIF withdrawal for 40 h in the presence of DMSO or 50 μM BMS-303141 (ACLi) and vehicle or 5 mM sodium acetate. **q**, Quantification of AP-positive colonies representing control and *Acly*-edited ES cells that failed to exit from the pluripotent state. ES cells were subjected to 2i/LIF withdrawal for 40 h in the presence of vehicle or 5 mM sodium acetate prior to reseeding at clonal density into medium containing 2i and LIF. Data are mean ± SD, $n = 5$ (**p**), $n = 4$ (**g, k, l**) or $n = 3$ (all other experiments) independent replicates. In **a–b**, significance was assessed using one-way ANOVA with Sidak's multiple comparisons post-test to compare total metabolite fraction labelled relative to control cells. In remaining panels, significance was assessed by two-way ANOVA relative to control cells (**k, q**) or DMSO treatment (**p**) with Sidak's multiple comparisons post-test, or by one-way ANOVA in comparison to control cells (**c, e, g**) with Sidak's multiple comparisons post-test or in the indicated comparisons (**l**) with Tukey's multiple comparisons post-test.



Extended Data Fig. 9 | Effect of SLC25A1 and MDH1 loss in exit from naive pluripotency. **a, b**, Relative viability (measured by PI exclusion) of control and *Slc25a1*-edited (left) and *Mdh1*-edited (right) ES cells maintained in the naive pluripotent state (+2i/LIF, **a**) or subjected to 2i/LIF withdrawal for 40 h (-2i/LIF, **b**). **c**, Steady-state levels of TCA cycle metabolites in control and *Slc25a1*-edited (left) and *Mdh1*-edited (right) ES cells subjected to 2i/LIF withdrawal for 40 h. Steady-state levels are represented as the fold change (expressed in log₂) relative to control cells. **d, e**, Relative O-propargyl-puromycin (OP-puro) mean fluorescence intensity (MFI) in control, *Slc25a1*-edited, *Acly*-edited and *Mdh1*-edited ES cells that have been maintained in the naive pluripotent state (**d**) or subjected to 2i/LIF withdrawal for 40 h (**e**). Dotted line represents

OP-puro MFI following cycloheximide (CHX) treatment as a control. **f, g**, Population doublings of control, *Slc25a1*-edited, *Acly*-edited and *Mdh1*-edited ES cells that have been maintained in the naive pluripotent state (**f**) or subjected to 2i/LIF withdrawal for 40 h (**g**). **h, i**, RT-qPCR of pluripotency-associated (*Nanog*, *Esrrb* and *Rex1*) and early differentiation-associated (*Sox1*) genes in control and *Slc25a1*-edited (**h**) and *Mdh1*-edited (**i**) ES cells subjected to 2i/LIF withdrawal for 40 h. Data are mean \pm SD, $n = 3$ independent samples. Significance was assessed in comparison to control cells by one-way ANOVA with Sidak's multiple comparisons post-test.



Extended Data Fig. 10 | Mode of TCA cycle engagement regulates cell fate.

a, Population doublings of control and *Aco2*-edited ES cells cultured in metastable (serum/LIF) conditions. **b**, Cumulative population doublings over the indicated passages of control and *Aco2*-edited ES cells upon conversion to the naive, ground state of pluripotency via addition of MEK and GSK3 β inhibitors (+2i). **c**, RT-qPCR of pluripotency-associated genes at the indicated passages in control and *Aco2*-edited ES cells following addition of 2i. Gene

expression at every passage was normalized to passage 0 (p0). Data are mean \pm SD, $n=1$ (**b**) or $n=3$ (**a, c**) independent replicates. Significance was assessed in comparison to control cells by one-way ANOVA with Sidak's multiple comparisons post-test (**a**) or relative to control cells at each timepoint with P values coloured according to comparison by two-way ANOVA with Sidak's multiple comparisons post-test (**c**).

Reporting Summary

Nature Research wishes to improve the reproducibility of the work that we publish. This form provides structure for consistency and transparency in reporting. For further information on Nature Research policies, see our [Editorial Policies](#) and the [Editorial Policy Checklist](#).

Statistics

For all statistical analyses, confirm that the following items are present in the figure legend, table legend, main text, or Methods section.

n/a Confirmed

- The exact sample size (n) for each experimental group/condition, given as a discrete number and unit of measurement
- A statement on whether measurements were taken from distinct samples or whether the same sample was measured repeatedly
- The statistical test(s) used AND whether they are one- or two-sided
 - Only common tests should be described solely by name; describe more complex techniques in the Methods section.*
- A description of all covariates tested
- A description of any assumptions or corrections, such as tests of normality and adjustment for multiple comparisons
- A full description of the statistical parameters including central tendency (e.g. means) or other basic estimates (e.g. regression coefficient) AND variation (e.g. standard deviation) or associated estimates of uncertainty (e.g. confidence intervals)
- For null hypothesis testing, the test statistic (e.g. F , t , r) with confidence intervals, effect sizes, degrees of freedom and P value noted
 - Give P values as exact values whenever suitable.*
- For Bayesian analysis, information on the choice of priors and Markov chain Monte Carlo settings
- For hierarchical and complex designs, identification of the appropriate level for tests and full reporting of outcomes
- Estimates of effect sizes (e.g. Cohen's d , Pearson's r), indicating how they were calculated

Our web collection on [statistics for biologists](#) contains articles on many of the points above.

Software and code

Policy information about [availability of computer code](#)

Data collection

Flow cytometry data was collected using a BD LSR Fortessa running FacsDiva (v8.0). Cell counts were collecting using a Beckman Multisizer 4e. Metabolite data was collected using an Agilent 7890A GC coupled to an Agilent 5977C mass selective detector or a Q Exactive HF-X Hybirdg Quadrupole-Orbitrap MS coupled to a Vanquish Flex Binary UHPLC system. Quantitative real-time PCR data was obtained using QuantStudio 5 or 6 Flex.

Data analysis

Flow cytometry analysis was performed using FCS Express (v7.04 and v7.05) or FlowJo (v10.8.0). Metabolite data was extracted and integrated using MassHunter software (vB.08). Correction for natural isotope abundance was performed using IsoCor (v1.0 or v2.0) software. Statistical tests were performed using GraphPad Prism v9.0.

Correlation modeling of DepMap data was performed with Python v3.8. To create the heatmap, the correlations were hierarchically clustered with the UPGMA algorithm using the `scipy.cluster.hierarchy.linkage` function from the SciPy Python package v1.4.1 . Network diagrams were created used Python package NetworkX v2.4 and Pygraphviz v0.13.2. Code corresponding to gene essentiality analysis is available at <https://github.com/finley-lab/coessentiality-network>.

RNA-seq libraries were filtered and trimmed using fastp v0.20.1 and mapped with STAR aligner v2.7.1a against the mm10 mouse genome assembly using default parameters. featureCounts v2.2.6 was used to calculate gene counts for input into DESeq2 v1.28.1 for quality control analysis, size normalization and variance dispersion corrections.

For manuscripts utilizing custom algorithms or software that are central to the research but not yet described in published literature, software must be made available to editors and reviewers. We strongly encourage code deposition in a community repository (e.g. GitHub). See the Nature Research [guidelines for submitting code & software](#) for further information.

Data

Policy information about [availability of data](#)

All manuscripts must include a [data availability statement](#). This statement should provide the following information, where applicable:

- Accession codes, unique identifiers, or web links for publicly available datasets
- A list of figures that have associated raw data
- A description of any restrictions on data availability

RNA-seq data that support the findings of this study have been deposited in the Gene Expression Omnibus under the accession code GSE183434. Alignment was performed against the mouse mm10 genome assembly. Gene essentiality data and NSCLC gene expression data are available from the DepMap Portal (<https://depmap.org/portal/>). Source data for Figs. 1–4 and Extended Data Figs. 1–10 are provided with the paper. Isotopologue distributions from all mass spectrometric isotope tracing experiments shown in the paper can be found in Supplementary Table 4.

Field-specific reporting

Please select the one below that is the best fit for your research. If you are not sure, read the appropriate sections before making your selection.

Life sciences Behavioural & social sciences Ecological, evolutionary & environmental sciences

For a reference copy of the document with all sections, see nature.com/documents/nr-reporting-summary-flat.pdf

Life sciences study design

All studies must disclose on these points even when the disclosure is negative.

Sample size	No statistical methods were used to predetermine sample size. Cell biology experiments were performed in triplicate or quadruplicate, which allowed us to detect statistically significant differences between groups/conditions (see: Naegle et al., <i>Science Signaling</i> 2015). The use of three replicates is considered standard practice in the field for ensuring reproducible results from cultured cells.
Data exclusions	No data were excluded.
Replication	All experiments were reliably reproduced. Each experiment was performed independently at least two times, but usually many more times.
Randomization	Samples were randomly distributed into groups.
Blinding	All data were collected and analyzed objectively using instruments without bias. Therefore, blinding is not relevant to this study.

Reporting for specific materials, systems and methods

We require information from authors about some types of materials, experimental systems and methods used in many studies. Here, indicate whether each material, system or method listed is relevant to your study. If you are not sure if a list item applies to your research, read the appropriate section before selecting a response.

Materials & experimental systems

n/a	Involved in the study
<input type="checkbox"/>	<input checked="" type="checkbox"/> Antibodies
<input type="checkbox"/>	<input checked="" type="checkbox"/> Eukaryotic cell lines
<input checked="" type="checkbox"/>	<input type="checkbox"/> Palaeontology and archaeology
<input checked="" type="checkbox"/>	<input type="checkbox"/> Animals and other organisms
<input checked="" type="checkbox"/>	<input type="checkbox"/> Human research participants
<input checked="" type="checkbox"/>	<input type="checkbox"/> Clinical data
<input checked="" type="checkbox"/>	<input type="checkbox"/> Dual use research of concern

Methods

n/a	Involved in the study
<input checked="" type="checkbox"/>	<input type="checkbox"/> ChIP-seq
<input type="checkbox"/>	<input checked="" type="checkbox"/> Flow cytometry
<input checked="" type="checkbox"/>	<input type="checkbox"/> MRI-based neuroimaging

Antibodies

Antibodies used

Antibodies used for western blotting in ESCs and C2C12s were: ACL (catalog no. 4332; Cell Signaling Technologies), ACO2 (catalog no. MA1-029; ThermoFisher), SLC25A1 (catalog no. 15235-1-AP; ProteinTech), MDH1 (catalog no. sc-166879; Santa Cruz Biotechnology), ACACA (catalog no. MAB6898; R&D Systems), AceCS1/ACSS2 (catalog no. 3658; Cell Signaling Technologies); TCF7L1 (catalog no. sc-166411; Santa Cruz Biotechnology), Myogenin/MYOG (catalog no. 14-5643-82; ThermoFisher), MYH3 (catalog no. 22287-1-AP; ProteinTech), Vinculin (catalog no. V9131; Sigma), Tubulin (catalog no. T9026; Sigma-Aldrich), H3K9ac (catalog no. 9469; Cell Signaling Technology), H3K14ac (catalog no. 07-353; Millipore Sigma), H3K27ac (catalog no. 39133; Active Motif), H4K16ac, (catalog no. 39167; Active Motif), H3 (catalog no. Ab1791; Abcam), and H4 (catalog no. 07-108; Millipore Sigma). Mouse (catalog no. NA931; Cytiva) and rabbit (catalog no. NA934; Cytiva) horseradish peroxidase-conjugated secondary antibodies were used.

Validation

Antibody validation was according to manufacturer's website and was as follows:
 ACL: Specificity was demonstrated by western blot of extracts from HeLa, NIH/3T3, C6 and COS cells.
 ACO2: Specificity was demonstrated by western blot of extracts from MCF7 cells transfected with Aco2-targeting siRNA (knockdown validated).
 SLC25A1: Specificity was demonstrated by western blot of extracts from HeLa, HepG2 and NCHI-H1299 cells.
 MDH1: Specificity was demonstrated by western blot of extracts from HeLa, K-562, EOC 20 and RAW 264 cells, among others.
 ACACA: Specificity was demonstrated by western blot of extracts from A431, HCT-116, HepG2 and C2C12 cells.
 AceCS1/ACSS2: Specificity was demonstrated by western blot of extracts from MCF7, HepG2, 293, NIH/373 and C2C12 cells, among others.
 MYOG: Specificity was demonstrated by western blot using extracts from cells with differential basal expression of MYOG; relative expression of MYOG was observed in RD and L6 lines relative to HEK-293 and NIH/3T3 cells.
 MYH3: Specificity was demonstrated by western blot of extracts from mouse embryo tissue.
 Vinculin: Specificity was demonstrated by western blot of extracts from HeLa, COS7, NIH/3T3, and CHO cells, among others.
 Tubulin: Specificity was demonstrated by western blot of extracts from HeLa, Jurkat, COS7, and NIH/3T3 cells, among others.
 H3K9ac: Specificity was demonstrated by western blot of extracts from HeLa and NIH/3T3 cells treated with trichostatin A.
 H3K14ac: Specificity was demonstrated by western blot of extracts from HeLa cells treated with sodium butyrate.
 H3K27ac: Specificity was demonstrated by western blot of nuclear extract from Raji cells treated with sodium butyrate.
 H4K16ac: Specificity was demonstrated by western blot of nuclear extract from HeLa cells treated with sodium butyrate.
 H3: Specificity was demonstrated by western blot of extracts from A431, Jurkat, or HEK293 cells +/- human histone H3 peptide.
 H4: Specificity was demonstrated by western blot of extract from HeLa cells.

Eukaryotic cell lines

Policy information about [cell lines](#)

Cell line source(s)

Mouse embryonic stem cells (ESCs) were previously generated from C57BL/6 × 129S4/SvJae F1 male embryos. C2C12, 143B, H2170, Calu-1 and H1395 cells were obtained from ATCC. Rex1::GFPd2 ESCs were a gift from Austin Smith, University of Exeter, United Kingdom (PMID: 21685889).

Authentication

Cell lines were not externally authenticated.

Mycoplasma contamination

Cell lines routinely tested negative for mycoplasma.

Commonly misidentified lines
(See [ICLAC](#) register)

No cell lines used in this study were found in the database of commonly misidentified cell lines that is maintained by ICLAC and NCBI Biosample.

Flow Cytometry

Plots

Confirm that:

- The axis labels state the marker and fluorochrome used (e.g. CD4-FITC).
- The axis scales are clearly visible. Include numbers along axes only for bottom left plot of group (a 'group' is an analysis of identical markers).
- All plots are contour plots with outliers or pseudocolor plots.
- A numerical value for number of cells or percentage (with statistics) is provided.

Methodology

Sample preparation

To prepare ESCs for viability assessment, media and PBS washes were collected along with cells removed from gelatin coated plates using Trypsin for 5 minutes at 37°C. Cells plus washes were then centrifuged and pellets were resuspended in FACS buffer containing PI (2.5 µg/mL) and analyzed by flow cytometry.

For Rex1::GFPd2 experiments, cells were washed with PBS and trypsinized prior to centrifugation. Pellets were resuspended in FACS buffer containing DAPI prior to analysis by flow cytometry.

For OP-puro experiments, cells were washed with PBS and trypsinized prior to centrifugation. Pellets were resuspended in PBS with eBioscience Fixable Viability Dye eFluor 450 (cat no. 65-0863014, Thermo Fisher Scientific) for 30 minutes. Cells were fixed in 4% PFA and permeabilized with 0.25% Triton-X-100 prior to staining of incorporated OP-Puro as indicated by manufacturer's protocol.

Instrument

BD LSR Fortessa

Software

FACSDiva was used for data acquisition. FCS Express (v7.04 and v7.05) or FlowJo (v10.8.0) was used for data analysis.

Cell population abundance

Clonal cell lines or homogenous cell populations were used for all experiments.

Gating strategy

For measuring viability: first, doublet exclusion was performed on cells gated by FSC-H versus FSC-W followed by SSC-H versus SSC-W. Debris was removed by excluding PI-negative and FSC-A low cells. Viable cells were identified by FSC-A and PI viability dye exclusion. For all other flow experiments: cells were separated from debris by FSC-A versus SSC-A. Then, doublet

exclusion was performed on cells gated by FSC-H versus FSC-W followed by SSC-H versus SSC-W. Viable cells were identified by FSC-A and DAPI or E450 fixable viability dye exclusion.

Tick this box to confirm that a figure exemplifying the gating strategy is provided in the Supplementary Information.